

IDENTIFICATION OF YOUNG STELLAR VARIABLES WITH KELT FOR K2 I: TAURUS DIPPERS AND ROTATORS

JOSEPH E. RODRIGUEZ¹, MEGAN ANSDELL², RYAN J. OELKERS³, PHILLIP A. CARGILE¹, ERIC GAIDOS^{4,5}, ANN MARIE CODY⁶, DANIEL J. STEVENS⁷, GARRETT SOMERS³, DAVID JAMES⁸, THOMAS G. BEATTY^{9,10}, ROBERT J. SIVERD¹¹, MICHAEL B. LUND³, RUDOLF B. KUHN¹², B. SCOTT GAUDI⁷, JOSHUA PEPPER¹³, KEIVAN G. STASSUN^{3,14}

¹Harvard-Smithsonian Center for Astrophysics, 60 Garden St, Cambridge, MA 02138, USA

²Institute for Astronomy, University of Hawai'i at Manoa, Honolulu, HI 96822, USA

³Department of Physics and Astronomy, Vanderbilt University, 6301 Stevenson Center, Nashville, TN 37235, USA

⁴Department of Geology and Geophysics, University of Hawai'i at Manoa, Honolulu, HI 96822

⁵Fulbright Fellow, Institute for Astrophysics, University of Vienna, Vienna AT-1180, Austria

⁶NASA Ames Research Center, Mountain View, CA 94035, USA

⁷Department of Astronomy, The Ohio State University, Columbus, OH 43210, USA

⁸Astronomy Department, University of Washington, Box 351580, Seattle, WA 98195, USA

⁹Department of Astronomy & Astrophysics, The Pennsylvania State University, 525 Davey Lab, University Park, PA 16802

¹⁰Center for Exoplanets and Habitable Worlds, The Pennsylvania State University, 525 Davey Lab, University Park, PA 16802

¹¹Las Cumbres Observatory Global Telescope Network, 6740 Cortona Dr., Suite 102, Santa Barbara, CA 93117, USA

¹²South African Astronomical Observatory, PO Box 9, Observatory 7935, South Africa

¹³Department of Physics, Lehigh University, 16 Memorial Drive East, Bethlehem, PA 18015, USA and

¹⁴Department of Physics, Fisk University, 1000 17th Avenue North, Nashville, TN 37208, USA

Draft version September 15, 2017

ABSTRACT

One of the most well-studied young stellar associations, Taurus-Auriga, was observed by the extended Kepler mission, K2, in the spring of 2017. K2 Campaign 13 (C13) is a unique opportunity to study many stars in this young association at high photometric precision and cadence. Using observations from the Kilodegree Extremely Little Telescope (KELT) survey, we identify “dippers”, aperiodic and periodic variables among K2 C13 target stars. This release of the KELT data (lightcurve data in e-tables) provides the community with long-time baseline observations to assist in the understanding of the more exotic variables in the association. Transient-like phenomena on timescales of months to years are known characteristics in the light curves of young stellar objects, making contextual pre- and post-K2 observations critical to understanding their underlying processes. We are providing a comprehensive set of the KELT light curves for known Taurus-Auriga stars in K2 C13. The combined data sets from K2 and KELT should permit a broad array of investigations related to star formation, stellar variability, and protoplanetary environments.

Subject headings: circumstellar matter, protoplanetary disks, stars: pre-main sequence, stars: variables: T Tauri

1. INTRODUCTION

The study of the photometric variability of young stellar objects (YSOs) goes back to the pioneering work of Joy (1949), who first associated variability in T Tauri stars (TTs) with the star formation process. Subsequent decades of photometric and spectroscopic investigations have painted a rich picture of the nature of TTs and their variability processes, which can include coherent periodic variations arising from surface star spots (akin to sunspots) as well as quasi-coherent and aperiodic variability arising from accretion and outflows, likely arising from magnetospheric interactions between the star and its protoplanetary disk (for an early comprehensive review, see Bertout 1989, and references therein). Additionally, TTs have shown variability, both short and long in duration, caused by circumstellar extinction from dust or part of the surrounding circumstellar disk (Herbst et al. 1994; Bouvier et al. 1999, 2013).

Therefore, studying the variability of TTs has been key to developing insight into the early stages of star formation, stellar angular momentum evolution, the

physics of magnetic star-disk interaction, and the nature of the protoplanetary gas and dust that lead to planet formation. With the success of long-time baseline surveys (All-Sky Automated Survey, Catalina Real-Time Transient Survey, and Palomar Transient Factory Pojmanski 1997; Drake et al. 2009; Law et al. 2009), the number of long-time baseline photometric observations of young stellar associations has significantly increased. From these long-time baseline, high-cadence observations, we are now able to study these systems in much greater detail.

As a result of observed spectroscopic signatures, TTs are typically split into two sub-groups, weak-lined T Tauri stars (WTTs) and classical T Tauri stars (CTTs). One key characteristic distinguishing the two sub-groups is the level of Balmer series H α emission observed in their optical spectra. CTTs have H α equivalent widths (EWs) $>5\text{--}10\text{\AA}$, whereas WTTs are more sedate ($\text{EW}_{\text{H}\alpha} \ll 5\text{\AA}$) in their emission (Martín et al. 1998; Barrado y Navascués & Martín 2003). However, this cutoff between CTTs and WTTs changes as a function of spectral type, and is closer to $>10\text{\AA}$ for M

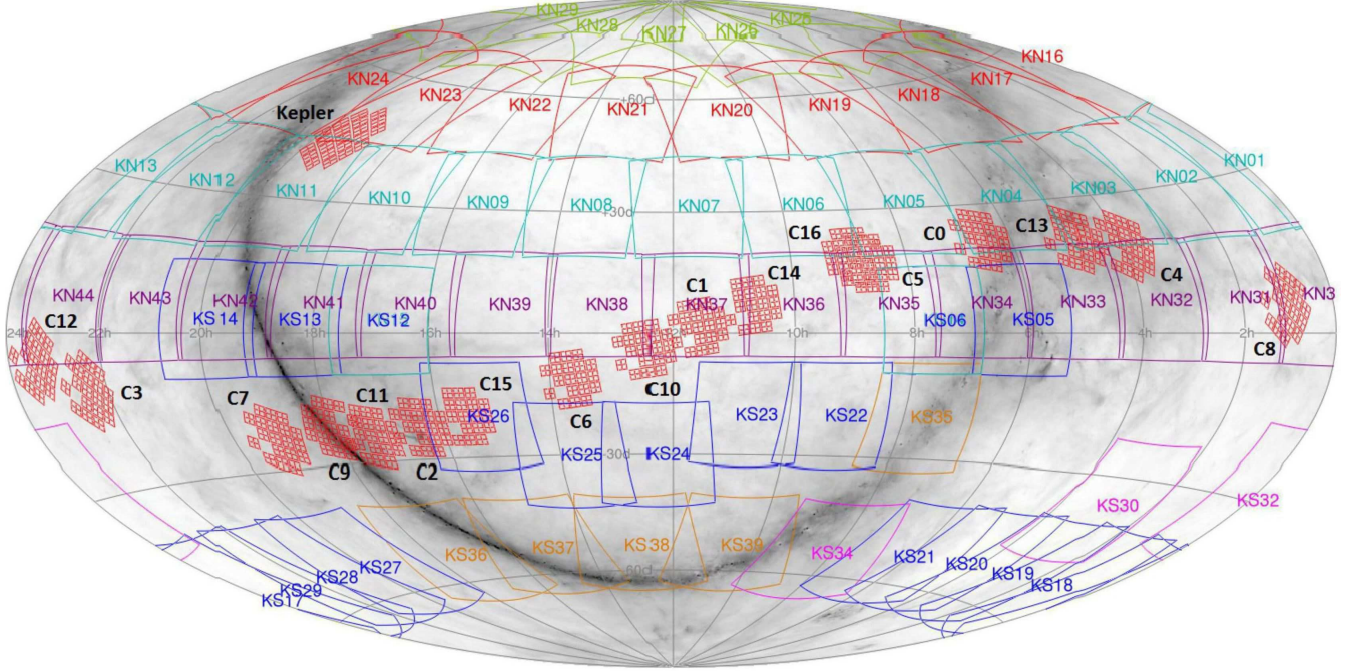


FIG. 1.— Map in celestial coordinates showing the locations of all of the KELT-North and KELT-South fields. The colors of each field indicates when the field was added to the normal observing scheme (Cyan: 2006; Blue: 2010; Red: 2012; Orange: 2013; Yellow: 2014). The purple equatorial fields were added in 2015 and only observed by KELT-North. The purple fields labeled KS34 and KS32 are the original KELT-South commissioning fields that were observed in 2009 and then added to the normal observing schedule in late-2011. The locations of the *Kepler* and *K2* fields are indicated by the red outline of each *Kepler* detector. This figure was created using the Montage Image Mosaic Engine (Berriman & Good 2017).

dwarfs (White & Basri 2003).

The variability for these two types of YSOs can also be quite different. WTTs tend to display relatively stable sinusoidal variability believed to be caused by surface star spots rotating in and out view (Stassun et al. 1999; Grankin et al. 2008; Rodríguez-Ledesma et al. 2009; Frasca et al. 2009). In contrast, CTTs display a wide variety of photometric variability which has been observed to be periodic, semi-periodic, or non-periodic (Herbst et al. 1994). The semi-periodic and periodic variability in CTTs has been attributed to circumstellar extinction (Herbst et al. 1994; Chelli et al. 1999; Alencar et al. 2010), occultations by an orbiting body in Keplerian motion (Mamajek et al. 2012; Bouvier et al. 2013; Rodríguez et al. 2013, 2016b), or accretion — either in a disk or onto the star (Bertout et al. 1988; Bertout 1989; Stassun et al. 1999; Carpenter et al. 2002; Scholz et al. 2009; Bouvier et al. 2007). Additionally, there is a new appreciation for a broad class of YSO variables that involve obscuration by disk material, referred to as “disk eclipsing” systems (see, e.g., Herbst et al. 2010; Plavchan et al. 2013; Rodríguez et al. 2015, 2016a, and references therein), whereby the star is occulted by features in its protoplanetary disk that may represent advanced stages of planet formation and that could provide a probe of protoplanetary material.

The Taurus-Aurigae association is the nearest (140 pc) and arguably the best-studied association of YSOs, in-

cluding the eponymous T Tauri stars, and their variability (see, e.g., Bertout 1989, and references therein as well as above). However, studying the variability of Taurus stars is challenging as the objects are spread over hundreds of square degrees. The advent of continuous, high-cadence, wide-field surveys has transformed our ability to comprehensively and systematically study these systems. The re-purposed *Kepler* mission, *K2* (Howell et al. 2014), has already supplied the community with high-precision photometry of the young stellar associations Upper Sco and ρ Oph (Ripepi et al. 2015; Ansdell et al. 2016b; Scaringi et al. 2016; Cody et al. 2017; Stauffer et al. 2017). Unfortunately, observations from *K2* are only taken in one band-pass, and the data are not available until months after they are taken. Thus, relying on those data alone limits our ability to identify and characterize variable stars of interest. Additionally, it is difficult to complement *K2* with simultaneous multi-wavelength observations. Multi-band photometric and spectroscopic observations can provide crucial information for identifying the sub-class of YSO variability. Therefore, to enable simultaneous *K2*-ground-based observations of variable young stars, we used photometric observations from the Kilodegree Extremely Little Telescope (KELT) survey to identify dippers and periodic signals of 56 YSOs in the Taurus-Auriga association. Of these, fifty of the stars in our sample were observed by *K2* during Cam-

paing 13. YSOs can display a wide range of variability, and the observing baseline, sky coverage, and precision of the KELT observations provide the unique ability to study these types of variability; from the short-duration events seen in dippers to the disk eclipsing systems that can dim for many months to years. We are releasing the results of our analysis and the corresponding data to extend the photometric time baseline of these targets, and enable complementary and simultaneous ground-based observations.

In this paper, we present time-series photometry from the KELT survey of known YSOs in the Taurus-Auriga association that were observed in K2 Campaign 13 (C13). Our target selection for this study is described in §2. The photometric observations are presented in §3. We present a robust estimate of the stellar parameters for each star in our sample and our methodology is shown in §4. We describe our technique for characterizing variability and periodicity in §5, overview the different identified variables in §6, and summarize our results in §7.

2. TARGET SELECTION

Taurus members were selected by combining the *Spitzer* infrared color-selected catalog of Luhman et al. (2010), which was in turn augmented with *WISE* data by Esplin et al. (2014), with the ultraviolet (UV)-selected catalog of Gómez de Castro et al. (2015), the Taurus Molecular Cloud sources identified as *Rosat* X-ray sources by Carkner et al. (1997), and the Taurus stars matched with X-ray sources from the *XMM-Newton* survey performed by Güdel et al. (2007). Only sources that had an infrared counterpart in either the 2MASS or *WISE* catalogs were retained. This concatenation produced 794 candidates, of which 295 were found to fall on working K2 detectors in C13.

Three stars have proper motions consistent with membership in the Hyades cluster and one star has a *Hipparcos* parallax identifying it as a foreground star. We excluded several other stars that have proper motions that deviate by more than 50 mas yr^{-1} from an iteratively-calculated median Taurus Molecular Cloud motion of $\mu_\alpha = +5 \text{ mas yr}^{-1}$, $\mu_\delta = -16 \text{ mas yr}^{-1}$, consistent with the motion found by Frink et al. (1997).

We estimated *Kepler* K_p magnitudes to select those stars sufficiently bright ($K_p < 19$) to detect the 10% flux variation over a day characteristic of “dipper” stars. This corresponds to $\leq 1\%$ photometric precision for K2 over 6.5 hr. K_p magnitudes were calculated using the most reliable method available, first with APASS or SDSS g and r magnitudes, using USNO-B B1 and R1 as a last resort. This final catalog contained 207 Taurus molecular cloud (TMC) members (median $K_p = 14.4$) and was then cross-matched to the KELT survey, resulting in 56 matches. However, due to the large pixel scale of the KELT telescopes some of these targets are blended in a single KELT lightcurve (see §4.1 for how blends were identified). The catalog broad-band magnitudes, kinematics, and estimated K_p magnitudes for these 56 sources are presented in Tables 1 and 2.

3. OBSERVATIONS: KELT

To identify variable YSOs among the Taurus YSOs prior to the K2 C13 observations (See Figure 1 for the K2 and KELT fields), we used observations from the KELT exoplanet transit survey. Designed to discover giant planets transiting bright ($V < 11$) host stars, the KELT survey uses two 42 mm telephoto lenses (KELT-North at Winer Observatory in Arizona in the United States and KELT-South at the South African Astronomical Observatory in Sutherland, South Africa). The two telescopes combine to observe over 70% of the entire sky with a 10-30 minute cadence. Each telescope setup provides a $26^\circ \times 26^\circ$ field of view and a $23''$ pixel scale. The typical photometric error for stars $7 < V < 11$ (the target brightness range) is $\sim 1\%$ but the telescopes also obtain lower precision observations of stars down to $V \sim 14$ (Pepper et al. 2007, 2012). Each KELT telescope uses a Paramount ME robotic German equatorial mount which requires a meridian flip when crossing from an east to west orientation. The east and west images are reduced and extracted separately. For a detailed description of the KELT observing strategy and data reduction process, see Siverd et al. (2012) and Kuhn et al. (2016). The light curves used in this work are from KELT-North field 03 which is centered at J2000 $\alpha = 03^h 58^m 12.0s$, $\delta = +31^\circ 39' 56.16''$ with the exception of J05080709+2427123 which is in KELT-North field 04 centered at J2000 $\alpha = 05^h 54^m 14.5s$, $\delta = +31^\circ 39' 56.16''$.

The per-point photometric error for our sample is dependent on the brightness of each target and ranges from 0.009 to 0.15 mag. Both KELT telescopes observe only with a non-standard broad R -band filter. Therefore, the reported KELT magnitudes in this paper do not correspond to any standard filter and are only instrumental magnitudes. All plots showing the KELT light curves are in relative magnitude where the median of the entire light curve has been subtracted off. The electronic tables being published with this paper report the KELT instrumental magnitudes and the corresponding instrumental per point error. The KELT light curves and catalog information for all 56 stars are publicly available as electronic table using a Filtergraph¹ portal (Burger et al. 2013).

We recommend only using KELT data where the relative flux uncertainty is $< 20\%$ rms.

4. IDENTIFYING VARIABLE AND PERIODIC OBJECTS

4.1. Variability Testing

We employed the following four variability metrics to determine the variability of objects in the Taurus field, following the work of Wang et al. (2013); Oelkers et al. (2015); and Oelkers et al. in prep (see Figure 2). These metrics help to identify large amplitude variability, which is not necessarily periodic. We outline each variability metric below but direct the reader to the previous works for a more detailed discussion of each metric. These metrics were determined empirically using all light curves in KELT-North field 03². Any star which passed all 4 metric cutoffs was flagged as a variable star.

¹ https://filtergraph.com/kelt_k2, This link includes KELT light curves for other papers in this series

² We use field 03 because all but one star were found in 03 and we do not expect much field-to-field variation for each metric

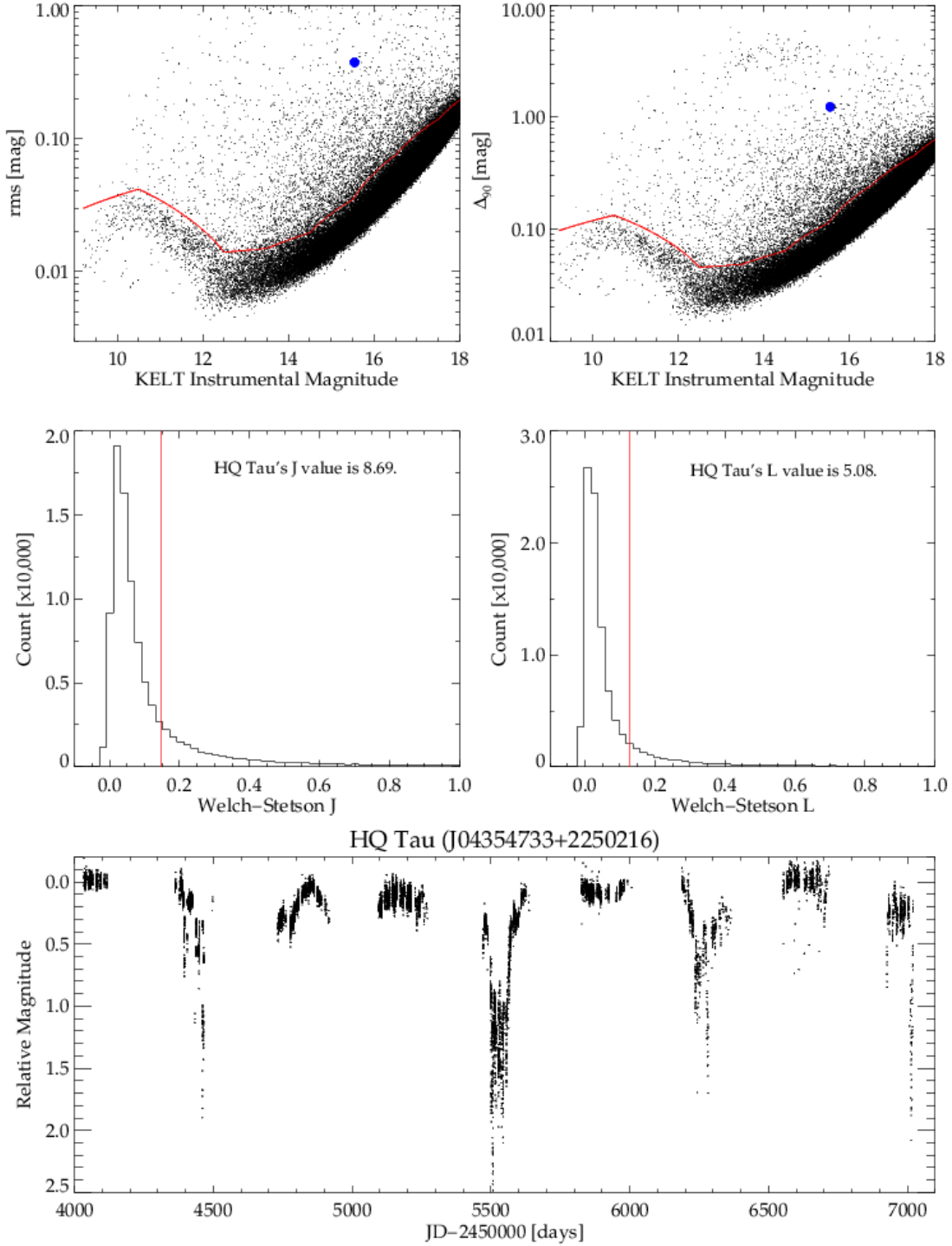


FIG. 2.— The variability metrics used to select K2 Taurus members as possible variable objects using the ensemble light curves found in KELT-North field 03. Stars lying above the red line in the top panels and to the right of the red line in the middle panels are expected to show variability due to astrophysical phenomena and not systematics. The cutoffs described below were calculated after an iterative 2.5σ clipping of the mean of each distribution to remove possible outliers. *Top Row:* The rms (left) and Δ_{90} (right) statistics and their respective, independent $+2\sigma$ quartiles shown as a red line. *Middle Row:* The Welch-Stetson J & L statistics and their respective $+3\sigma_J$ & $+5\sigma_L$ cuts, calculated using objects with $J, L < 3$ and a 2.5σ iterative clipping process. We find the KELT-North field 03 has a distribution of J values with a mean value of 0.054 ± 0.031 , leading to a cut of 0.147; and a distribution of L values with a mean of 0.033 ± 0.019 , leading to a cut of 0.128. *Bottom Row:* The light curve of HQ Tau. HQ Tau passed all 4 variability metrics and is identified as statistically variable. The star is shown as a blue dot in the top panels and its J & L values are labeled in the middle panels.

Additionally, we flagged any star as a possible blend if another star has a magnitude within 1.5 of the target star's magnitude and is located within $2' (\sim 5 \text{ pix})$.

First we identify stars with light curves that show un-

usually high dispersion for their magnitude, using the rms and Δ_{90} statistics. The rms statistic identifies the magnitude range for 68% of the data points in each light curve; the Δ_{90} statistics identifies the magnitude range

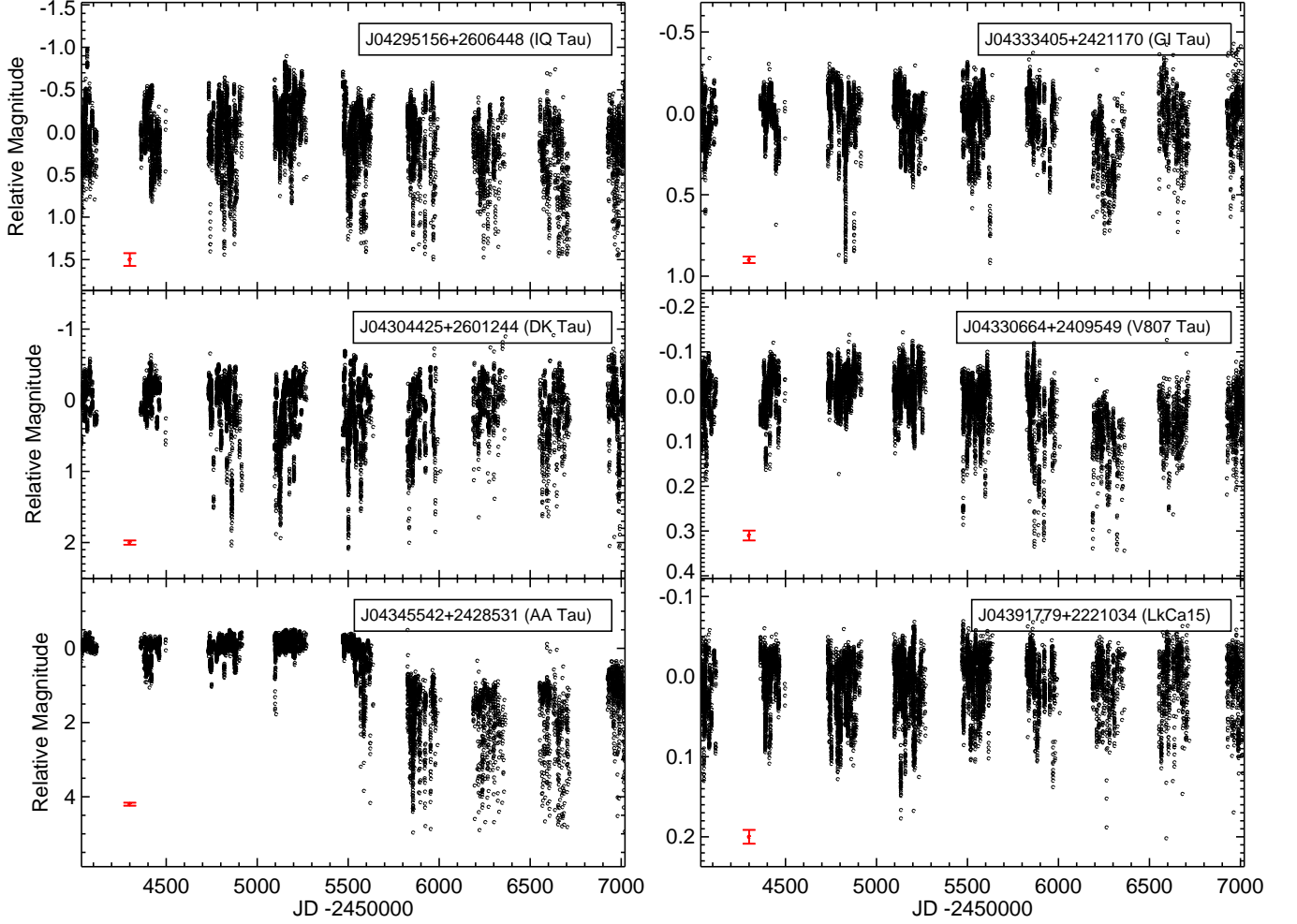


FIG. 3.— The KELT light curves for the six dipper stars identified in our sample. The median per-point error is shown on the bottom left of each plot in red.

for 90% of the data points in each light curve. We compute the upper 2σ envelopes of both statistics individually, as a function of magnitude, and assume an object is lying above these limits because of *bona-fide* astrophysical variability. These statistics were not calculated with error weighting but because we wanted the envelopes to be based on stars with no apparent light curve variation, we applied an iterative 2.5σ clipping to the sample, as a function of magnitude, prior to re-calculating the final 2σ envelope of each metric.

Next we compute the Welch-Stetson J and L statistics (Stetson 1996). These two statistics are useful to compute the variability between subsequent data points on the sampling rate of the KELT survey, typically 10–30 min. These statistics are expected to produce a distribution of values centered at or near zero with a one-sided tail. Stars in this tail are expected to be variable. We remove objects with $J, L > 3$ and do a 2.5σ iterative clipping to determine the mean and standard deviation of the J & L distributions prior to determining the cut-offs described below. This clipping allows us to calculate the distribution properties of J & L using a population of stars which show minimal light curve variation. The Stetson J & L values are shown in Table 3.

Finally, we applied a $+3\sigma$ cutoff of this tail in J and the

$+5\sigma_J$ cutoff of this tail in L to select variable objects. We applied a $+5\sigma_L$ cutoff in L , rather than $+3\sigma_L$ cutoff, because we found the larger limit helped to remove spurious objects which passed the first 3 metrics but showed features of known detector systematics while retaining objects that show variation consistent with astrophysical phenomena.

4.2. Periodicity Testing

Following the approach of Stassun et al. (1999), we also executed a search for periodic signals using a Lomb-Scargle (L-S) periodogram (Lomb 1976; Scargle 1982). We searched for periods between a minimum period of 0.5 days and a maximum period of 50 days using 2000 frequency steps. Additionally, we masked periods between 0.5 and 0.505 d and 0.97–1.04 d to avoid the most common detector aliases associated with the solar and sidereal day and selected the highest peak of the power spectrum as the candidate period.

We then executed a boot-strap analysis, using 1000 Monte-Carlo iterations, where the dates of the observations were not changed but the magnitude values of the light curve were randomly scrambled (see Henderson & Stassun 2012). We recalculated the Lomb-Scargle power spectrum for each iteration and recorded

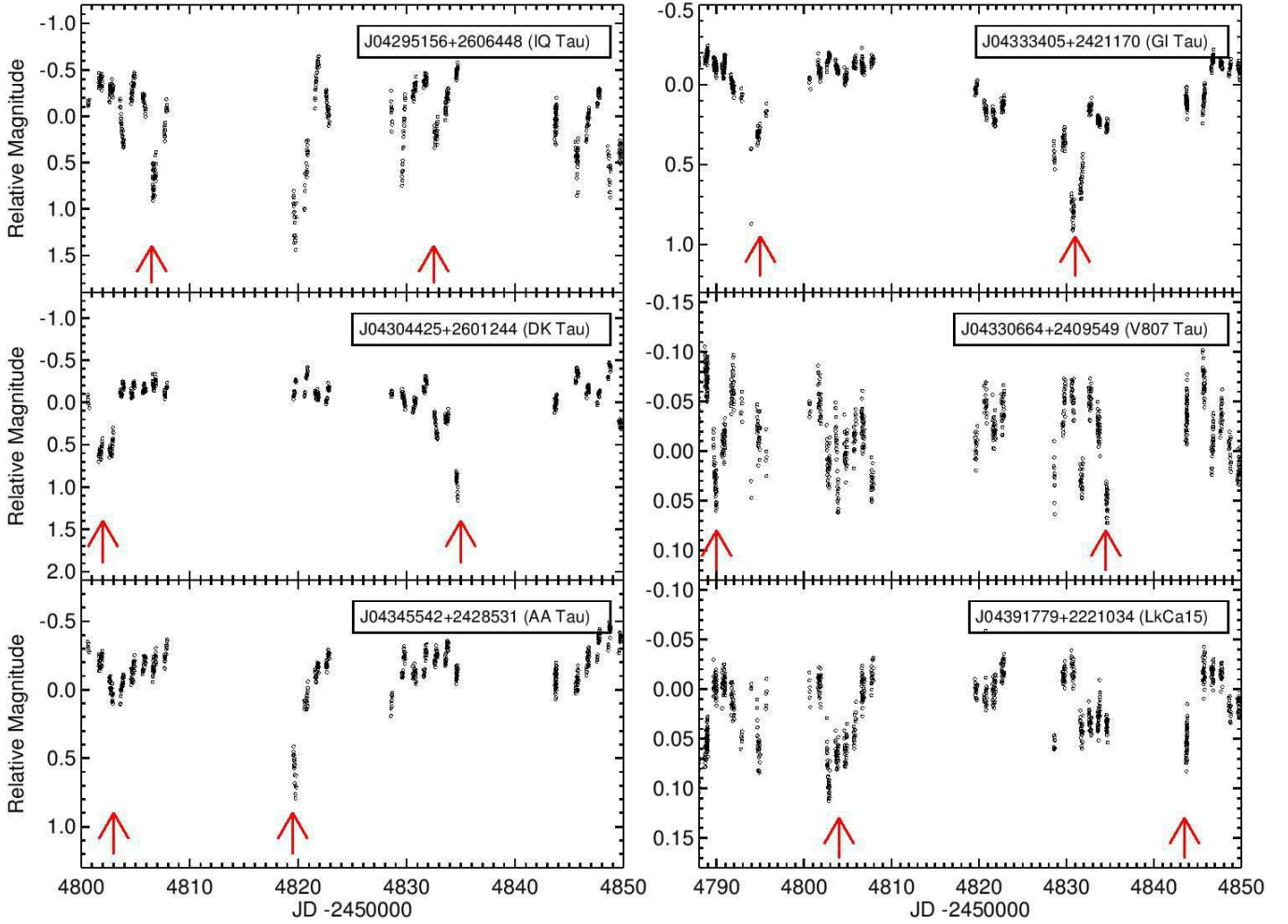


FIG. 4.— A zoom in on the six dippers identified showing the dipper phenomena at various depths. The arrows are marking some representative dips for each dipper, not necessarily all of them.

the maximum peak power. If, after 1000 iterations, a maximum power of the boot-strap analysis was found to be larger than the power of the candidate period, the period was rejected as a false-positive.

The top periodic signals found for each target using the technique described here are listed in Table 3 and the corresponding phase folded light curve is shown in Figures 5 and 6. In general we interpret the periodic signals to likely be the rotation period of the primary star. A full interpretation of each individual case is beyond the scope of this paper.

5. INTERESTING VARIABLES

In this section, we identify the interesting variable objects in our sample and summarize their properties based on the existing literature. This information will aid future follow-up observations of these targets and support the analysis of the K2 C13 photometry.

5.1. Dippers and UXORs

Some YSOs, known as “dippers”, display short-duration large-amplitude dimmings that may be related to planet formation (Cody & Hillenbrand 2010; Cody et al. 2014). This sub-class of YSOs consists of T Tauri stars with optical light curves that exhibit very

deep (~ 10 – 60% in flux) and short-duration (~ 0.5 – 2 day) dimming events that are consistent with large dusty structures orbiting in the inner disk and transiting our line-of-sight to the star (e.g. Morales-Calderón et al. 2011; Cody et al. 2014; Ansdell et al. 2016b). The flux dips can occur either quasi-periodically or aperiodically; when the dips are quasi-periodic, their periods are often similar to the stellar rotation period, suggesting that the occulting material is co-rotating with the star (e.g. Ansdell et al. 2016b; Bodman et al. 2016). Although it was initially thought that dipper stars host nearly edge-on disks (e.g., McGinnis et al. 2015), the handful of dippers with outer disk inclinations measured directly from resolved images exhibit a range of orientations, including face-on, intermediate, and nearly edge-on inclinations (Ansdell et al. 2016a; Scaringi et al. 2016). The disks around dipper stars are in the early stages of planet formation, and these systems provide a unique probe of inner disk conditions during planet formation.

Another type of YSO with possible planet formation implications is UX Orionis (UXOR) stars, intermediate-mass pre-main sequence (PMS) stars (typically Herbig Ae stars) that also exhibit very deep dimming events that last for many months (see review in Waters & Waelkens 1998). It is unclear whether dippers

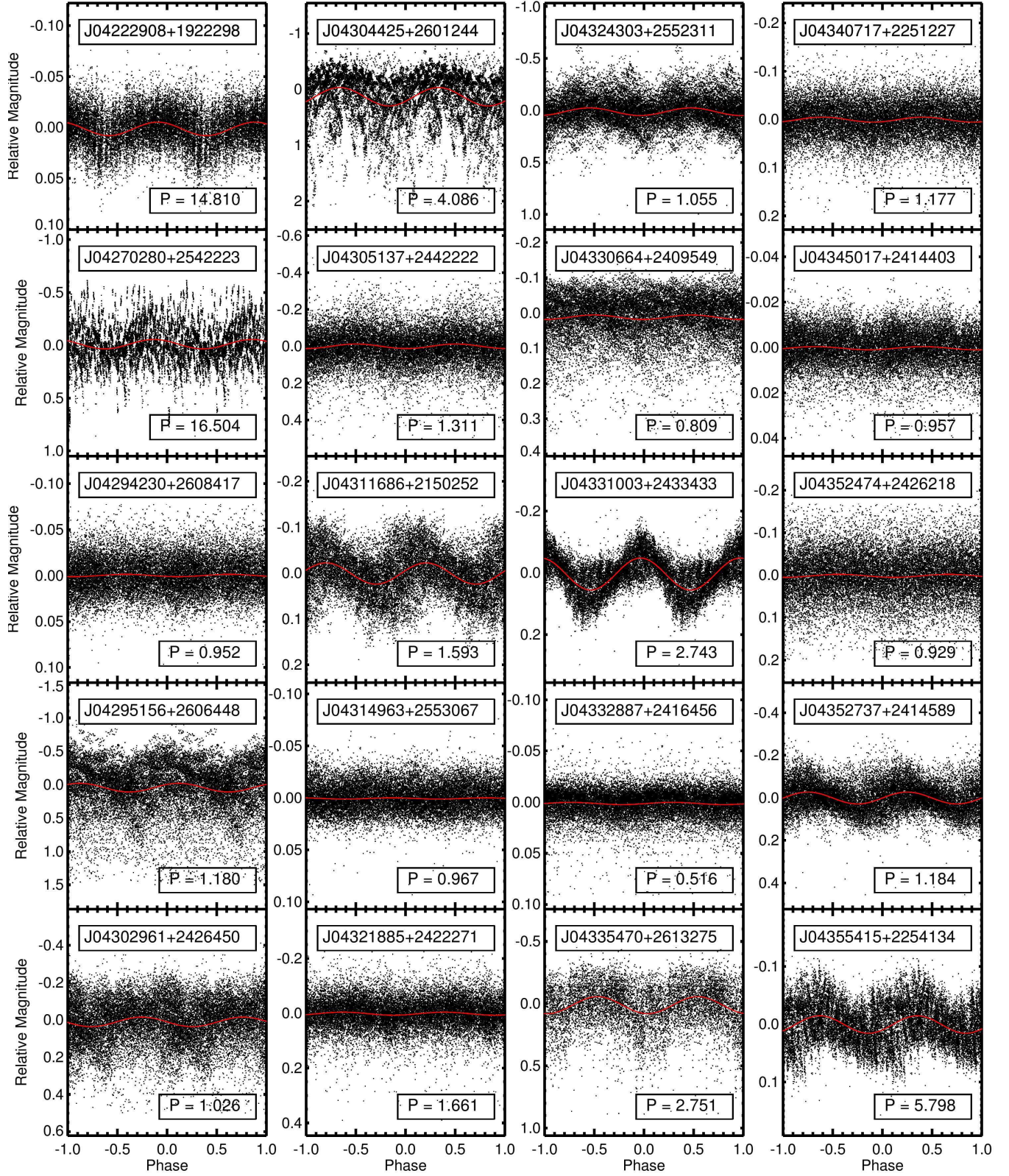


FIG. 5.— The KELT light curves for the identified periodic variables. The red line corresponds a sinusoidal fit to the phase-folded KELT observations.

and UXORs are produced by the same physical mechanism(s); but both classes of objects are thought to be related to occultations of the star by dusty circumstellar material. However, in contrast to lower-mass dippers,

the dimming events of UXORs typically occur aperiodically and last weeks to months (Grinin et al. 1991). It has been proposed that the UXOR dimming could be caused by hydrodynamical fluctuations of the inner-disk rim

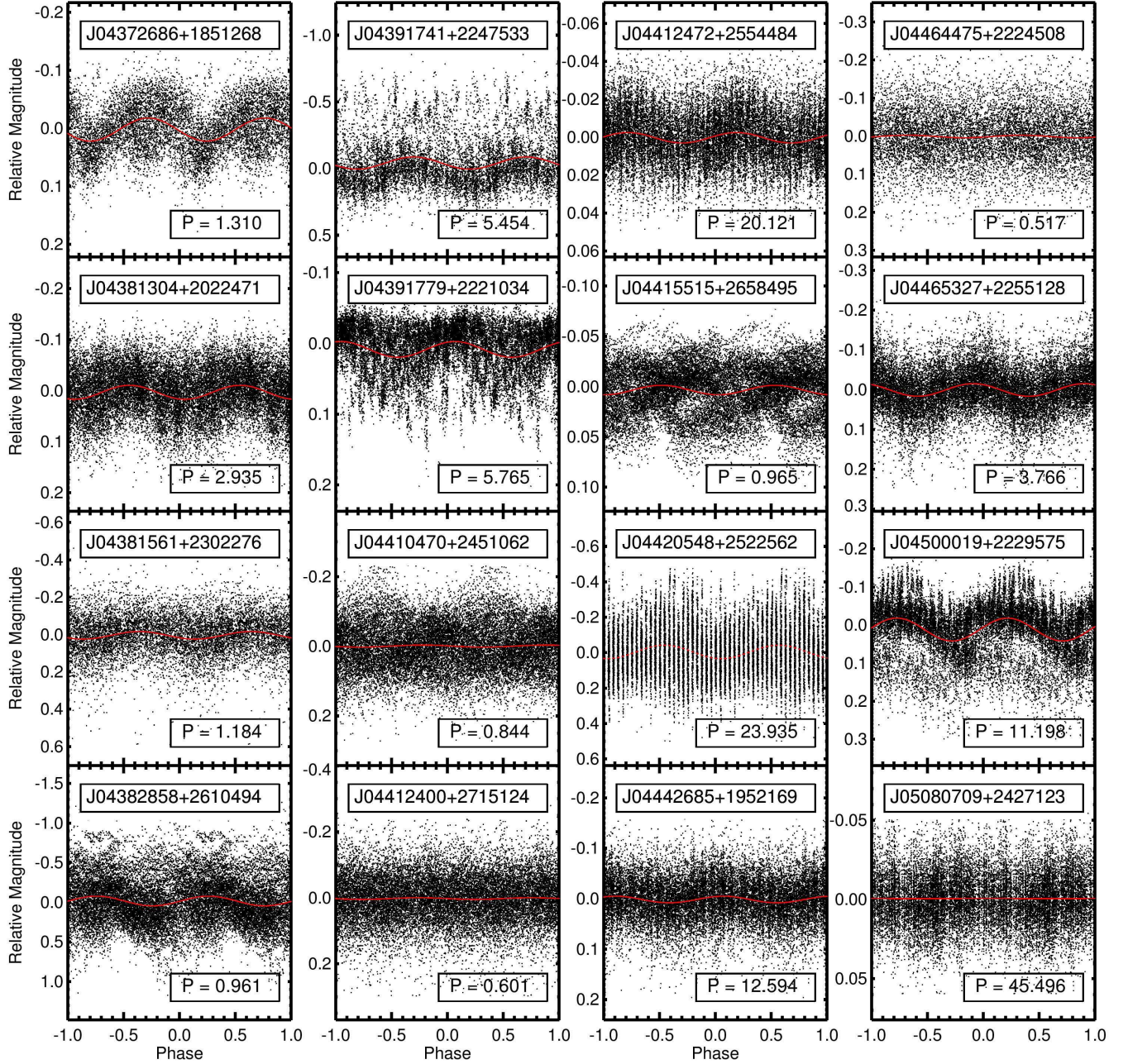


FIG. 6.— Figure 5 (continued): The KELT light curves for the identified periodic variables. The red line corresponds a sinusoidal fit to the phase-folded KELT observations.

(Dullemond et al. 2003). Time-series multi-pass-band photometry, spectroscopy, and polarimetry can provide information on the gas and dust components of occulting material. For example, UXOR dimming is accompanied by an increase in polarization as well as a color reversal (i.e., initial reddening and subsequent blue-ing), consistent with extinction by dust.

To classify dippers in our sample, we visually analyzed the KELT light curves for short duration (< 2 days), deep (~ 10 – 60% in flux) dimming events. From this search, we identified six dippers and one UXOR star. The UXOR (HQ Tau) and one of the dippers (AA Tau) were previously identified in the literature. All of these sources have protoplanetary disks con-

firmed with sub-mm continuum observations. We summarize their properties below and provide their full light curves in Figures 2 and 3. A zoom in of the dipper phenomena for the six identified dippers is shown in Figure 4. Any dipper that also shows periodicity in their light curve is shown again in Figures 5 and 6.

5.1.1. AA Tau (J04345542+2428531)

AA Tau is the prototypical dipper. Its photometric variability was originally characterized by Bouvier et al. (1999) and the system has been extensively monitored in the several decades since its discovery (e.g. Bouvier et al. 2003, 2007, 2013; Zhang et al. 2015; Rodriguez et al. 2015). Apart from its dipper behav-

ior, AA Tau is a fairly typical T Tauri star: it has a K7 spectral type, is a single star, and hosts a protoplanetary disk (e.g., Bouvier et al. 1999; Nguyen et al. 2012; Andrews et al. 2013). The system has an accretion rate of $\log \dot{M}_* = -8.48 \text{ } M_{\odot} \text{ yr}^{-1}$ and its protoplanetary disk has a dust mass of $M_{\text{dust}} \approx 30 M_{\oplus}$ (Najita et al. 2015). The disk also has a high inclination and is seen nearly edge-on (Ménard et al. 2003; Cox et al. 2013).

The optical light curve of AA Tau shows a constant maximum brightness $V \approx 12.5$ mag, punctuated by regular dimming events every 8.2 days, where the dimming varied in depth but was typically ~ 1.5 magnitudes. The dimming events have been interpreted as occultations of the central star by an inner disk warp located at a few stellar radii, where the inner disk warp is produced by interactions between an inclined stellar magnetosphere and a nearly edge-on accretion disk (Bouvier et al. 1999). In 2011, AA Tau suddenly dimmed by ~ 2 mags in V -band and the regular flux dips were no longer detectable. The sudden enhanced extinction may be related to outer disk material coming into our line-of-sight as a result of Keplerian rotation or magnetic buoyancy instability (Bouvier et al. 2013; Rodriguez et al. 2015; Zhang et al. 2015).

The KELT data of AA Tau have been previously published in Rodriguez et al. (2015), and we refer to this paper for a detailed analysis of the light curve. In short, the KELT data recovers the photometric characteristics of AA Tau reported previously in the literature and summarized above, in particular its ~ 8 -day period and the sudden dimming in 2011. However, the reported ~ 8 -day periodicity is only recovered in individual KELT seasons, and not found when running the L-S periodogram on the entire nine seasons of KELT data, thus we do not report a period for AA Tau in Table 3. Note that the increase in photometric scatter seen in the KELT observations after the 2011 dimming of AA Tau (see Figure 3) is due to the system being near the faintness limit of the telescope.

5.1.2. LkCa 15 (J04391779+2221034)

LkCa 15 is a single star of K5 spectral type with an accretion rate of $\log \dot{M}_* = -8.87 \text{ } M_{\odot} \text{ yr}^{-1}$ (Najita et al. 2015). It hosts a massive protoplanetary disk with $M_{\text{dust}} \approx 60 M_{\oplus}$ (Najita et al. 2015; see also Andrews et al. 2013; Kraus et al. 2012) at an intermediate inclination of $\sim 50^\circ$ (e.g., Andrews et al. 2011; Thalmann et al. 2014). The disk is a so-called “transitional disk” (TD) with a large inner dust gap extending to ~ 50 AU at sub-mm wavelengths (Andrews et al. 2011). Kraus & Ireland (2012) have also identified a possible forming protoplanet orbiting inside the dust gap using non-redundant aperture masking interferometry. However, recent observations of LkCa 15 with SPHERE have found no evidence of a protoplanet (Thalmann et al. 2016).

The KELT-North data show a rotational signal at $P \approx 5.7$ days superimposed with aperiodic drops in flux of ~ 0.15 mag (see Figure 5). Although the dust cavity seen in the sub-mm may seem to contradict the dipper behavior, LkCa 15 is known to host an inner disk that could be providing the occulting dust. Its strong NIR excess, similar to the median SED of Taurus disks, in-

dicates the presence of a compact and optically thick inner disk component near the dust sublimation radius (Espaillat et al. 2010). Additionally, VLT/SPHERE images have resolved disk material in scattered light from 7–30 AU, which likely represents the optically thin regions of the inner disk component (Thalmann et al. 2015).

5.1.3. IQ Tau (J04295156+2606448)

IQ Tau has an M0.5 spectral type and exhibits an accretion rate of $\log \dot{M}_* = -7.55 \text{ } M_{\odot} \text{ yr}^{-1}$ (Najita et al. 2015). The source hosts a protoplanetary disk with $M_{\text{dust}} \approx 30 M_{\oplus}$ (Andrews et al. 2013; Williams & Best 2014; Najita et al. 2015) and appears to be a single star based on high-resolution near-IR imaging (Daemgen et al. 2015) and high-resolution spectroscopy (Nguyen et al. 2012). The inclination of IQ Tau’s disk has been estimated from sub-mm continuum and line emission to be $\sim 58^\circ$ (Guilloteau et al. 2014).

The KELT-North data show a periodic signal of $P \approx 1.2$ days superimposed with aperiodic drops in brightness of up to ~ 1 mag (see Figure 5). This period is not consistent with the $P = 6.25$ day signal found by Bouvier et al. (1995).

5.1.4. DK Tau (J04304425+2601244)

DK Tau is a K8+M1 binary system with a separation of ~ 350 AU (Akeson & Jensen 2014; Andrews et al. 2013). The primary hosts a disk with $M_{\text{dust}} \approx 12 M_{\oplus}$ at an inclination of $41 \pm 11^\circ$, while the secondary hosts a disk with $M_{\text{dust}} \approx 2.0 M_{\oplus}$ at an inclination of $70 \pm 13^\circ$ (Akeson & Jensen 2014). The system is also clearly accreting with $\log \dot{M}_* = -7.42 \text{ } M_{\odot} \text{ yr}^{-1}$ (Najita et al. 2015).

The KELT-North data show a periodic signal at $P \approx 4.1$ days, superimposed with deep aperiodic dips up to ~ 2 mag in depth (see Figure 5). Bouvier et al. (1995) found a rotational period of 8.4 days, which we also recover but at lower signal-to-noise. DK Tau has been previously identified as a UXOR candidate by Oudmaijer et al. (2001), who used optical broadband photo-polarimetry to identify sources with significant photometric variability as well as increased polarization during dimming. In particular, while observing DK Tau over two days, they found a dimming of $V \sim 1$ mag accompanied by a doubling of the polarization from 1 to 2%. However, our more extensive KELT-North data show that the dimming events last only a few days, which is more akin to dipper rather than UXOR behavior (See Figures 3 and 4).

5.1.5. GI Tau (J04333405+2421170)

GI Tau is a K7 star that hosts a protoplanetary disk with a relatively low dust mass of $M_{\text{dust}} \approx 5 M_{\oplus}$ but a high accretion rate of $\log \dot{M}_* = -7.69 \text{ } M_{\odot} \text{ yr}^{-1}$ (Najita et al. 2015). The disk inclination has not yet been directly constrained (e.g., by resolved imaging). It appears to be a single star based on high-resolution near-IR imaging (Daemgen et al. 2015) and high-resolution spectroscopy (Nguyen et al. 2012).

The KELT-North light curve exhibits dimming events that can be up to ~ 1 mag in depth (see Figure 3

and 4). We do not find a significant period, however Bouvier et al. (1995) found a rotation period of 7.2 days.

5.1.6. V807 Tau (J04330664+2409549)

V807 Tau is a well-characterized triple system (see Schaefer et al. 2012, and references therein). The two wider components are separated by ~ 300 mas, with the secondary being itself a binary with a ~ 40 mas separation. Schaefer et al. (2012) used spatially resolved high-resolution spectra to determine that the primary has a K7 spectral type while the secondary is an M2-M2 binary. Moreover, their SED analysis showed IR excess consistent with an accretion disk around only the primary component of the system; there are no disk signatures for the secondary component. Andrews et al. (2013) measured a composite sub-mm continuum flux consistent with $M_{\text{dust}} \approx 4M_{\oplus}$.

The KELT-North light curve exhibits a period of $P \approx 0.8$ days, superimposed with aperiodic ~ 0.2 mag drops in brightness (see Figure 5). The components of the triple system are unresolved in the KELT photometry, however the dips are unlikely to be caused by the stellar companions.

5.1.7. HQ Tau (J04354733+2250216)

HQ Tau has a K2 spectral type and hosts a protoplanetary disk with a relatively low dust mass of $M_{\text{dust}} \approx 2M_{\oplus}$ (Andrews et al. 2013). The disk inclination has not yet been directly constrained (e.g., by resolved imaging). The source appears to be a single star based on high-resolution imaging (Simon et al. 1995) and high-resolution spectroscopy (Nguyen et al. 2012).

Using Super-WASP photometry, Norton et al. (2007) recovered a periodic signal of $P = 2.4546$ days for HQ Tau, which we recover in the first and fourth KELT-North seasons. However, because we do not recover a period when running the L-S periodogram on the entire nine seasons of KELT data, we do not report a period for HQ Tau in Table 3. The second, fifth, and seventh KELT-North seasons show extended dimming events characteristic of UXOR variables: the dimming events reach ~ 1.5 -mag depths and last for weeks to months (See Figure 2). UXOR behavior for this star has been previously reported in Watson et al. (2015).

5.2. Long-term Dimming

Two sources in our sample exhibit long-term dimming events that last for years. It is unclear whether these dimming events are related to circumstellar material or stellar variability.

5.2.1. V1334 Tau (J04445445+2717454)

V1334 Tau has a reported K1 spectral type (Wichmann et al. 1996), but is also a multiple system that includes a close binary at $\sim 0.1''$ separation with $\Delta K \approx 2$ mag (Daemgen et al. 2015). The system has been classified as a WTTS based on its low $H\alpha$ emission (Wichmann et al. 1996) and lacks the IR excess that would be indicative of a protoplanetary disk.

A full analysis of the KELT-North data for V1334 Tau has been presented in Rodriguez et al. (2017). In short, the KELT-North light curve shows a long-duration dimming event of ~ 0.12 mag beginning in 2009, which to

date has not ended. Additionally, a ~ 0.32 day periodicity was observed in every KELT season. It remains unclear what mechanisms are causing the long-term dimming and ~ 0.32 day periodicity; see Rodriguez et al. (2017) for a discussion of possible interpretations.

5.2.2. V1341 Tau (J04500019+2229575)

V1341 Tau has a K1 spectral type and has been classified as a WTTS based on its low $H\alpha$ emission (Wichmann et al. 1996). It shows no evidence (e.g., IR excess) of a significant protoplanetary disk. V1341 Tau has candidate companions at $2.1''$ and $8.4''$ with ΔK values of 4.45 and 4.72, respectively (Daemgen et al. 2015). The source gradually dims across all nine KELT-North seasons by ~ 0.3 mags in total. We do not recover a significant periodic signal in any of the KELT seasons; the full light curve for this target is shown in Figure 7.

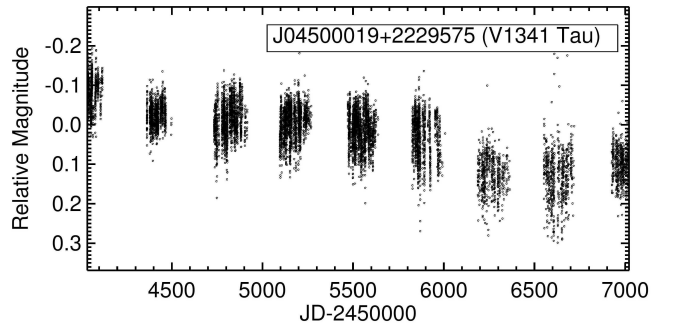


FIG. 7.— The KELT lightcurve for the long-term variable J04500019+2229575 (V1341 Tau).

5.3. Aperiodic Variability

Here we present the targets in our sample that display photometric variability, often super-imposed on a periodic signal. These sources tend to have very high accretion rates, which is consistent with the observed photometric nature seen in their light curves. The phase-folded KELT light curves for sources with detected periodicity are shown in Figures 5 and 6.

5.3.1. DF Tau (J04270280+2542223)

DF Tau is an M2.0-M2.5 binary at 99 ± 14 mas separation, with both components classified as CTTs based on spectroscopic indicators (Hartigan & Kenyon 2003). The unresolved system is detected in the sub-mm continuum with a composite flux that corresponds to $M_{\text{dust}} \approx 2M_{\oplus}$ in aggregate (Andrews et al. 2013). Both components have particularly high accretion rates of $\log M_* = -6.9 M_{\odot} \text{yr}^{-1}$ (Hartigan & Kenyon 2003).

The KELT-North data show a periodicity of $P \approx 16.5$ days. The periodic signal appears to be superimposed on accretion driven variability, as shown in Figure 5. Our measured period differs from that of Bouvier et al. (1995), who monitored DF Tau with ground-based *UVBRI* photometry and found a tentative period of 9.8 days with their *U*-band light curves only.

The nature of DF Tau's photometric variability is consistent with the accretion state of this object. In particular, DF Tau is thought to be in an unstable ac-

cretion regime based on the persistence of the redshifted absorption component in its H δ Balmer line (see Kurosawa & Romanova 2013, and references therein). In this regime, matter is thought to accrete along several transient accretion streams that appear in random locations, producing a aperiodic photometric light curve.

5.3.2. *CI Tau* (J04335200+2250301)

CI Tau has a K7 spectral type and hosts a massive protoplanetary disk with $M_{\text{dust}} \approx 60 M_{\oplus}$ (Andrews et al. 2013). Resolved images reveal an extended disk with a weak non-axisymmetric feature (Kwon et al. 2015). The system exhibits a notably high accretion rate of $\log \dot{M}_* = -6.8 M_{\odot} \text{yr}^{-1}$ (Hartigan et al. 1995), consistent with the photometric variability seen in its KELT-North light curve.

The KELT-North data do not show a significant periodic signal. However, Johns-Krull et al. (2016) found a tentative rotational period of ~ 7.1 days based on 14 nights of ground-based V-band measurements. Variability in optical spectra has also been detected, which was interpreted as a temporary obscuration of a local hot region by circumstellar material (Smith et al. 1999).

This system was recently found to have a candidate young massive planet based on radial velocity (RV) variations in the optical and IR (Johns-Krull et al. 2016). The RV amplitude yields $M \sin i \sim 8 M_{\text{Jup}}$, which, in conjunction with a disk inclination of $\approx 46^\circ$ estimated from sub-mm continuum emission (Guilloteau et al. 2014), corresponds to a planet mass of $\sim 11\text{--}12 M_{\text{Jup}}$.

5.3.3. *DN Tau* (J04352737+2414589)

DN Tau is a CTTS with an M0 spectral type. It hosts a massive protoplanetary disk with $M_{\text{dust}} \approx 45 M_{\oplus}$ (Andrews et al. 2013) at an inclination of $\sim 30^\circ$ (Guilloteau et al. 2014) based on sub-mm continuum and line images. DN Tau has a fairly high accretion rate of $\log \dot{M}_* = -8.45 M_{\odot} \text{yr}^{-1}$ (e.g., Gullbring et al. 1998), although this is lower than the other sources in this subclass.

We recover a period of $P \approx 1.184$ days in the KELT-North data, with non-periodic variability superimposed over the periodic signal (see Figure 5). This period is not consistent with the previous estimate of a ~ 6 day rotation period by Bouvier et al. (1995).

5.3.4. *DO Tau* (J04382858+2610494)

DO Tau is a CTTS with an M0 spectral type. It hosts a massive protoplanetary disk with $M_{\text{dust}} \approx 50 M_{\oplus}$ (Andrews et al. 2013), and resolved images reveal a compact disk with an inclination of $\sim -32^\circ$ (Kwon et al. 2015). The system has a notably high accretion rate of $\log \dot{M}_* = -6.84 M_{\odot} \text{yr}^{-1}$ (Gullbring et al. 1998), consistent with the variability seen in its KELT-North light curve. We recover a periodic signal of ≈ 0.96 days in the KELT-North data. However Osterloh et al. (1996) found a rotational period of 12.5 ± 1.8 days while monitoring the system over 10 days at optical wavelengths.

5.3.5. *V999 Tau* (J04420548+2522562)

V999 Tau is an M0.5-M2.5 binary separated by $0.27''$. The secondary in V999 Tau has a fairly

high accretion rate of $\log \dot{M}_* = -8.24 M_{\odot} \text{yr}^{-1}$, while the primary has an upper limit of $\log \dot{M}_* = -8.58 M_{\odot} \text{yr}^{-1}$ (Hartigan & Kenyon 2003). V1000 Tau (J04420732+2523032) and V995 Tau (J04420777+2523118) are both blended with the V999 Tau binary in the KELT-North data. However, we find a significant periodic signal of $P \approx 23.9$ days, which appears to be superimposed with non-periodic variability, as shown in Figure 5.

5.3.6. *UZ Tau* (J04324303+2552311 & J04324282+2552314)

UZ Tau is a quadruple system with UZ Tau Eab about $4''$ away from UZ Tau Wab. UZ Tau E is an M1-M4 single-lined spectroscopic binary (Mathieu et al. 1996; Prato et al. 2002), while UZ Tau W is an M2-M3 sub-arcsecond binary separated by $0.34''$ (Hartigan & Kenyon 2003). UZ Tau E has a very high accretion rate of $\log \dot{M}_* = -5.7$ (Hartigan et al. 1995), while both components in UZ Tau B also have high accretion rates of $\log \dot{M}_* = -8.0 M_{\odot} \text{yr}^{-1}$ (Hartigan & Kenyon 2003), again consistent with the variability seen in their KELT-North lightcurve.

In the KELT-North data, we recover a periodic signal with $P \approx 1.06$ days as shown in Figure 5. The recovered periodicity matches the period of the UZ Tau E spectroscopic binary. However, as this quadruple system is unresolved in the KELT data, the light curve should be interpreted with caution.

6. SUMMARY AND CONCLUSION

In this paper, we have identified and visually classified the light curves of 56 YSOs in Taurus that were observed by the extended *Kepler* mission, K2 during Campaign 13. Using observations from the KELT survey, we have identified six dippers (five previously unknown), a previously known UXor, six aperiodic variables, and two stars displaying long duration dimming events. Additionally, we use a L-S periodicity search on all the stars in our sample and identify any targets that display periodic variability. Table 2 reports the top L-S period recovered that is not a known alias and Figures 5 and 6 show the phase-folded KELT light curves.

KELT observations provide long-time baseline (≤ 10 years), high-cadence (10-30 min) photometry that is well-suited to studying both the short- and long-duration photometric variability of YSOs. The upcoming *Transiting Exoplanet Survey Satellite* (TESS, Ricker et al. 2014), will obtain high-precision photometric observations of almost the entire sky for a duration of ≥ 27 days. Many young stellar associations are expected to be observed during the TESS mission. Similar to the work presented here, observations from ground-based surveys can complement the upcoming TESS campaigns by extending the observing time baseline by a decade or more. We encourage the community to use the identified variables from our analysis to obtain targeted simultaneous and/or complementary observations, such as multi-band photometry and time-series spectroscopy, to better understand the underlying processes causing the observed variability and their relation to planet formation.

The data published with this paper are intended to provide a legacy data set to complement the very high-precision photometric observations of these targets by

K2. We are providing the KELT light curves for known Taurus-Auriga stars in K2 C13 (UT 2017 Mar 08 to UT 2017 May 27) with this paper. The KELT and K2 photometry, combined with ground-based multi-band photometry and spectroscopy, will provide a comprehensive data set to study the underlying astrophysical processes related to star formation, stellar variability, and protoplanetary environments.

Early work on KELT-North was supported by NASA Grant NNG04GO70G. J.A.P. and K.G.S. acknowledge support from the Vanderbilt Office of the Provost through the Vanderbilt Initiative in Data-intensive Astrophysics. This work has made use of NASA's Astrophysics Data System and the SIMBAD database operated at CDS, Strasbourg, France. Work performed by

J.E.R. was supported by the Harvard Future Faculty Leaders Postdoctoral fellowship. Work performed by P.A.C. was supported by NASA grant NNX13AI46G. Work by K.G.S. was supported by NSF PAARE grant AST-1358862. Work by D.J.S. and B.S.G. was partially supported by NSF CAREER Grant AST-1056524. G.S. acknowledges the support of the Vanderbilt Office of the Provost through the Vanderbilt Initiative in Data-intensive Astrophysics (VIDA) fellowship.

This research made use of Montage. It is funded by the National Science Foundation under Grant Number ACI-1440620, and was previously funded by the National Aeronautics and Space Administration's Earth Science Technology Office, Computation Technologies Project, under Cooperative Agreement Number NCC5-626 between NASA and the California Institute of Technology.

REFERENCES

- Akeson, R. L., & Jensen, E. L. N. 2014, *ApJ*, 784, 62
- Alam, S., Albareti, F. D., Allende Prieto, C., et al. 2015, *ApJS*, 219, 12
- Alencar, S. H. P., Teixeira, P. S., Guimarães, M. M., et al. 2010, *A&A*, 519, A88
- Andrews, S. M., Rosenfeld, K. A., Kraus, A. L., & Wilner, D. J. 2013, *ApJ*, 771, 129
- Andrews, S. M., Wilner, D. J., Espaillat, C., et al. 2011, *ApJ*, 732, 42
- Ansdell, M., Gaidos, E., Williams, J. P., et al. 2016a, *MNRAS*, 462, L101
- Ansdell, M., Gaidos, E., Rappaport, S. A., et al. 2016b, *ApJ*, 816, 69
- Barrado y Navascués, D., & Martín, E. L. 2003, *AJ*, 126, 2997
- Berriman, G. B., & Good, J. C. 2017, *ArXiv e-prints*, arXiv:1702.02593
- Bertout, C. 1989, *ARA&A*, 27, 351
- Bertout, C., Basri, G., & Bouvier, J. 1988, *ApJ*, 330, 350
- Bodman, E. H. L., Quillen, A. C., Ansdell, M., et al. 2016, *ArXiv e-prints*, arXiv:1605.03985
- Bouvier, J., Covino, E., Kovo, O., et al. 1995, *A&A*, 299, 89
- Bouvier, J., Grankin, K., Ellerbroek, L. E., Bouy, H., & Barrado, D. 2013, *A&A*, 557, A77
- Bouvier, J., Chelli, A., Allain, S., et al. 1999, *A&A*, 349, 619
- Bouvier, J., Grankin, K. N., Alencar, S. H. P., et al. 2003, *A&A*, 409, 169
- Bouvier, J., Alencar, S. H. P., Boutelier, T., et al. 2007, *A&A*, 463, 1017
- Burger, D., Stassun, K. G., Pepper, J., et al. 2013, *Astronomy and Computing*, 2, 40
- Carkner, L., Mamajek, E., Feigelson, E., et al. 1997, *ApJ*, 490, 735
- Carpenter, J. M., Hillenbrand, L. A., Skrutskie, M. F., & Meyer, M. R. 2002, *AJ*, 124, 1001
- Chelli, A., Carrasco, L., Mújica, R., Recillas, E., & Bouvier, J. 1999, *A&A*, 345, L9
- Cody, A. M., & Hillenbrand, L. A. 2010, *ApJS*, 191, 389
- Cody, A. M., Hillenbrand, L. A., David, T. J., et al. 2017, *ApJ*, 836, 41
- Cody, A. M., Stauffer, J., Baglin, A., et al. 2014, *AJ*, 147, 82
- Cox, A. W., Grady, C. A., Hammel, H. B., et al. 2013, *ApJ*, 762, 40
- Cutri, R. M., & et al. 2014, *VizieR Online Data Catalog*, 2328, 0
- Cutri, R. M., Skrutskie, M. F., van Dyk, S., et al. 2003, *VizieR Online Data Catalog*, 2246, 0
- Daemgen, S., Bonavita, M., Jayawardhana, R., Lafrenière, D., & Janson, M. 2015, *ApJ*, 799, 155
- Drake, A. J., Djorgovski, S. G., Mahabal, A., et al. 2009, *ApJ*, 696, 870
- Dullemond, C. P., van den Ancker, M. E., Acke, B., & van Boekel, R. 2003, *ApJ*, 594, L47
- Espaillat, C., D'Alessio, P., Hernández, J., et al. 2010, *ApJ*, 717, 441
- Esplin, T. L., Luhman, K. L., & Mamajek, E. E. 2014, *ApJ*, 784, 126
- Frasca, A., Covino, E., Spezzi, L., et al. 2009, *A&A*, 508, 1313
- Frink, S., Röser, S., Neuhauser, R., & Sterzik, M. F. 1997, *A&A*, 325, 613
- Gaia Collaboration, Brown, A. G. A., Vallenari, A., et al. 2016, *ArXiv e-prints*, arXiv:1609.04172
- Gómez de Castro, A. I., López-Santiago, J., López-Martínez, F., et al. 2015, *ApJS*, 216, 26
- Grankin, K. N., Bouvier, J., Herbst, W., & Melnikov, S. Y. 2008, *A&A*, 479, 827
- Grinin, V. P., Kiselev, N. N., Chernova, G. P., Minikulov, N. K., & Voshchinnikov, N. V. 1991, *Ap&SS*, 186, 283
- Güdel, M., Padgett, D. L., & Dougados, C. 2007, *Protostars and Planets V*, 329
- Guilloteau, S., Simon, M., Piétu, V., et al. 2014, *A&A*, 567, A117
- Gullbring, E., Hartmann, L., Briceño, C., & Calvet, N. 1998, *ApJ*, 492, 323
- Hartigan, P., Edwards, S., & Ghandour, L. 1995, *ApJ*, 452, 736
- Hartigan, P., & Kenyon, S. J. 2003, *ApJ*, 583, 334
- Henderson, C. B., & Stassun, K. G. 2012, *ApJ*, 747, 51
- Herbst, W., Herbst, D. K., Grossman, E. J., & Weinstein, D. 1994, *AJ*, 108, 1906
- Herbst, W., LeDuc, K., Hamilton, C. M., et al. 2010, *AJ*, 140, 2025
- Howell, S. B., Sobek, C., Haas, M., et al. 2014, *PASP*, 126, 398
- Johns-Krull, C. M., McLane, J. N., Prato, L., et al. 2016, *ApJ*, 826, 206
- Joy, A. H. 1949, *ApJ*, 110, 424
- Kraus, A. L., & Ireland, M. J. 2012, *ApJ*, 745, 5
- Kraus, A. L., Ireland, M. J., Hillenbrand, L. A., & Martinache, F. 2012, *ApJ*, 745, 19
- Kuhn, R. B., Rodriguez, J. E., Collins, K. A., et al. 2016, *MNRAS*, 459, 4281
- Kurosawa, R., & Romanova, M. M. 2013, *MNRAS*, 431, 2673
- Kwon, W., Looney, L. W., Mundy, L. G., & Welch, W. J. 2015, *ApJ*, 808, 102
- Law, N. M., Kulkarni, S. R., Dekany, R. G., et al. 2009, *PASP*, 121, 1395
- Lomb, N. R. 1976, *Ap&SS*, 39, 447
- Luhman, K. L., Allen, P. R., Espaillat, C., Hartmann, L., & Calvet, N. 2010, *ApJS*, 186, 111
- Mamajek, E. E., Quillen, A. C., Pécaut, M. J., et al. 2012, *AJ*, 143, 72
- Martin, E. L., Montmerle, T., Gregorio-Hetem, J., & Casanova, S. 1998, *MNRAS*, 300, 733
- Mathieu, R. D., Martin, E. L., & Magazzu, A. 1996, in *Bulletin of the American Astronomical Society*, Vol. 28, American Astronomical Society Meeting Abstracts #188, 920
- McGinnis, P. T., Alencar, S. H. P., Guimarães, M. M., et al. 2015, *A&A*, 577, A11
- Ménard, F., Bouvier, J., Dougados, C., Mel'nikov, S. Y., & Grankin, K. N. 2003, *A&A*, 409, 163
- Morales-Calderón, M., Stauffer, J. R., Hillenbrand, L. A., et al. 2011, *ApJ*, 733, 50
- Najita, J. R., Andrews, S. M., & Muzerolle, J. 2015, *MNRAS*, 450, 3559
- Nguyen, D. C., Brandeker, A., van Kerkwijk, M. H., & Jayawardhana, R. 2012, *ApJ*, 745, 119
- Norton, A. J., Wheatley, P. J., West, R. G., et al. 2007, *A&A*, 467, 785
- Oelkers, R. J., Macri, L. M., Wang, L., et al. 2015, *AJ*, 149, 50
- Osterloh, M., Thommes, E., & Kania, U. 1996, *A&AS*, 120, 267
- Oudmaijer, R. D., Palacios, J., Eiroa, C., et al. 2001, *A&A*, 379, 564
- Pepper, J., Kuhn, R. B., Siverd, R., James, D., & Stassun, K. 2012, *PASP*, 124, 230
- Pepper, J., Pogue, R. W., DePoy, D. L., et al. 2007, *PASP*, 119, 923
- Plavchan, P., Güth, T., Laohakunakorn, N., & Parks, J. R. 2013, *A&A*, 554, A110
- Pojmanski, G. 1997, *Acta Astronomica*, 47, 467
- Prato, L., Simon, M., Mazeh, T., Zucker, S., & McLean, I. S. 2002, *ApJ*, 579, L99

- Ricker, G. R., Winn, J. N., Vanderspek, R., et al. 2014, in *Proc. SPIE*, Vol. 9143, *Space Telescopes and Instrumentation 2014: Optical, Infrared, and Millimeter Wave*, 914320
- Ripepi, V., Balona, L., Catanzaro, G., et al. 2015, *MNRAS*, 454, 2606
- Rodríguez, J. E., Pepper, J., Stassun, K. G., et al. 2013, *AJ*, 146, 112
- . 2015, *The Astronomical Journal*, 150, 32
- Rodríguez, J. E., Stassun, K. G., Cargile, P., et al. 2016a, *ApJ*, 831, 74
- Rodríguez, J. E., Reed, P. A., Siverd, R. J., et al. 2016b, *AJ*, 151, 29
- Rodríguez, J. E., Zhou, G., Cargile, P. A., et al. 2017, *ArXiv e-prints*, arXiv:1701.03044
- Rodríguez-Ledesma, M. V., Mundt, R., & Eislöffel, J. 2009, *A&A*, 502, 883
- Scargle, J. D. 1982, *ApJ*, 263, 835
- Scaringi, S., Manara, C. F., Barenfeld, S. A., et al. 2016, *MNRAS*, 463, 2265
- Schaefer, G. H., Prato, L., Simon, M., & Zavala, R. T. 2012, *ApJ*, 756, 120
- Scholz, A., Xu, X., Jayawardhana, R., et al. 2009, *MNRAS*, 398, 873
- Simon, M., Ghez, A. M., Leinert, C., et al. 1995, *ApJ*, 443, 625
- Siverd, R. J., Beatty, T. G., Pepper, J., et al. 2012, *ApJ*, 761, 123
- Skrutskie, M. F., Cutri, R. M., Stiening, R., et al. 2006, *AJ*, 131, 1163
- Smith, K. W., Lewis, G. F., Bonnell, I. A., Bunclark, P. S., & Emerson, J. P. 1999, *MNRAS*, 304, 367
- Stassun, K. G., Mathieu, R. D., Mazeh, T., & Vrba, F. J. 1999, *AJ*, 117, 2941
- Stauffer, J., Collier Cameron, A., Jardine, M., et al. 2017, *AJ*, 153, 152
- Stetson, P. B. 1996, *PASP*, 108, 851
- Thalmann, C., Mulders, G. D., Hodapp, K., et al. 2014, *A&A*, 566, A51
- Thalmann, C., Mulders, G. D., Janson, M., et al. 2015, *ApJ*, 808, L41
- Thalmann, C., Janson, M., Garufi, A., et al. 2016, *ApJ*, 828, L17
- Wang, L., Macri, L. M., Wang, L., et al. 2013, *AJ*, 146, 139
- Waters, L. B. F. M., & Waelkens, C. 1998, *ARA&A*, 36, 233
- Watson, C., Henden, A. A., & Price, A. 2015, *VizieR Online Data Catalog*, 1
- White, R. J., & Basri, G. 2003, *ApJ*, 582, 1109
- Wichmann, R., Krautter, J., Schmitt, J. H. M. M., et al. 1996, *A&A*, 312, 439
- Williams, J. P., & Best, W. M. J. 2014, *ApJ*, 788, 59
- Zhang, K., Crockett, N., Salyk, C., et al. 2015, *ApJ*, 805, 55

TABLE 1

2MASS ID	EPIC ID	RA J2000 (Degrees)	DEC J2000 (Degrees)	pmRA (mas yr ⁻¹)	pmDE (mas yr ⁻¹)	K _p mag	u'	g'	r'	i'	z'	Gaia Parallax ¹
J04222908+1922298	210767482	65.62122028	19.37491611	10.50	-37.30	10.68	N/A ± N/A	N/A ± N/A	N/A ± N/A	N/A ± N/A	N/A ± N/A	10.76 ± 0.227
J04270280+2542223	247986526	66.76162028	25.70621667	12.82	-19.09	11.32	15.517 ± 0.017	11.888 ± 0.001	11.004 ± 0.001	10.344 ± 0.001	10.109 ± 0.001	N/A ± N/A
J04274793+2430121	247813679	66.94972111	24.50334556	5.40	-5.50	11.73	15.567 ± 0.008	15.176 ± 0.011	11.661 ± 0.001	11.192 ± 0.001	13.21 ± 0.013	N/A ± N/A
J04294230+2608417	248045033	67.42626917	26.14492889	13.90	-15.20	11.31	15.27 ± 0.008	12.236 ± 0.001	11.3 ± 0.001	10.912 ± 0.001	11.357 ± 0.002	N/A ± N/A
J04295156+2606448	248040905	67.46482694	26.11245611	17.90	-33.60	13.54	17.123 ± 0.01	15.622 ± 0.008	13.069 ± 0.002	12.13 ± 0.002	12.808 ± 0.013	N/A ± N/A
J04302961+2426450	247805410	67.62340861	24.44584083	6.10	-18.50	13.02	16.637 ± 0.007	15.332 ± 0.005	13.258 ± 0.003	12.081 ± 0.001	12.744 ± 0.011	N/A ± N/A
J04303292+2602440	248032266	67.63719472	26.04559417	5.80	-11.00	13.09	16.214 ± 0.007	16.287 ± 0.015	13.101 ± 0.001	12.75 ± 0.001	13.997 ± 0.018	N/A ± N/A
J04304153+2430416	247814868	67.67311806	24.51152583	16.80	-31.30	12.80	16.467 ± 0.008	16.171 ± 0.015	12.8 ± 0.001	12.13 ± 0.002	13.647 ± 0.013	N/A ± N/A
J04304425+2601244	248029373	67.6843475	26.02351472	1.50	-22.00	12.21	17.245 ± 0.027	14.056 ± 0.001	15.612 ± 0.012	14.669 ± 0.011	13.672 ± 0.013	N/A ± N/A
J04305137+2442222	247843485	67.7141225	24.70620778	7.90	-17.80	13.85	16.459 ± 0.007	15.511 ± 0.005	13.768 ± 0.003	12.205 ± 0.001	11.482 ± 0.003	N/A ± N/A
J04305171+2441475	247842020	67.715473	24.696531	3.00	-21.00	18.64	N/A ± N/A	N/A ± N/A	N/A ± N/A	N/A ± N/A	N/A ± N/A	N/A ± N/A
J04311686+2150252	247454835	67.82024222	21.84035556	2.10	-13.50	10.68	N/A ± N/A	N/A ± N/A	N/A ± N/A	N/A ± N/A	N/A ± N/A	8.038 ± 0.259
J04314963+2553067	248010721	67.95685056	25.88520778	7.63	-40.31	9.73	11.246 ± 0.001	10.125 ± 0.001	9.632 ± 0.001	9.51 ± 0.001	10.536 ± 0.003	7.968 ± 0.362
J04321786+2422149	247794636	68.074424	24.370829	0.00	-16.00	17.79	N/A ± N/A	N/A ± N/A	N/A ± N/A	N/A ± N/A	N/A ± N/A	N/A ± N/A
J04321885+2422271	247795097	68.078635	24.37419667	6.60	-19.70	13.45	18 ± 0.012	15.367 ± 0.004	14.772 ± 0.011	15.841 ± 0.014	12.619 ± 0.011	N/A ± N/A
J04324282+2552314	248009353	68.17839361	25.87536611	0.00	0.00	12.06	16.423 ± 0.008	15.651 ± 0.006	12.383 ± 0.001	11.291 ± 0.002	11.505 ± 0.005	N/A ± N/A
J04324303+2552311	248009353	68.17939917	25.87528556	0.00	0.00	12.06	16.423 ± 0.008	15.651 ± 0.006	12.383 ± 0.001	11.291 ± 0.002	11.505 ± 0.005	N/A ± N/A
J04330664+2409549	247764745	68.27763417	24.16528306	10.50	-20.40	10.95	15.164 ± 0.006	12.28 ± 0.001	12.253 ± 0.002	11.166 ± 0.001	10.532 ± 0.002	N/A ± N/A
J04331003+2433433	247822311	68.29179167	24.56200889	3.60	-21.40	11.93	15.9 ± 0.006	13.438 ± 0.002	11.652 ± 0.001	11.02 ± 0.001	10.977 ± 0.002	N/A ± N/A
J04332887+2416456	247781229	68.37035361	24.27931194	23.37	-17.71	7.87	9.569 ± 0.001	8.327 ± 0.001	7.753 ± 0.001	7.754 ± 0.001	9.149 ± 0.002	N/A ± N/A
J04333405+2421170	247792225	68.39192028	24.35474806	-3.00	-15.60	13.03	24.355 ± 0.628	24.774 ± 0.511	22.489 ± 0.144	21.148 ± 0.066	21.801 ± 0.391	N/A ± N/A
J04333456+2421058	247791801	68.39401333	24.35163028	0.00	0.00	12.72	16.537 ± 0.008	15.991 ± 0.013	12.357 ± 0.001	14.176 ± 0.012	12.957 ± 0.011	N/A ± N/A
J04335200+2250301	247584113	68.4667325	22.84169556	11.90	-15.40	12.57	15.808 ± 0.007	14.066 ± 0.002	12.404 ± 0.001	11.691 ± 0.001	13.036 ± 0.013	N/A ± N/A
J04335470+2613275	248055184	68.47815389	26.22436333	34.20	-11.30	13.87	18.587 ± 0.017	16.034 ± 0.005	16.589 ± 0.016	15.396 ± 0.014	14.337 ± 0.015	N/A ± N/A
J04335562+2425016	247801362	68.48175194	24.41711667	3.90	-4.10	13.41	22.072 ± 0.58	20.642 ± 0.095	19.202 ± 0.041	18.203 ± 0.028	17.09 ± 0.032	N/A ± N/A
J04340717+2251227	247585953	68.525991	22.85627306	7.30	-25.60	12.17	N/A ± N/A	N/A ± N/A	N/A ± N/A	N/A ± N/A	N/A ± N/A	N/A ± N/A
J04342961+2423421	247798120	68.62335278	24.39502833	-9.10	-0.90	12.75	20.471 ± 0.102	18.999 ± 0.017	17.662 ± 0.008	17.009 ± 0.007	16.825 ± 0.019	N/A ± N/A
J04345017+2414403	247776236	68.70904833	24.24452139	23.93	-18.76	8.95	14.064 ± 0.009	9.735 ± 0.001	8.821 ± 0.001	8.558 ± 0.001	9.62 ± 0.003	5.299 ± 0.235
J04345542+2428531	247810494	68.73091556	24.48140444	4.30	-15.30	13.72	15.86 ± 0.008	13.937 ± 0.002	12.206 ± 0.001	11.492 ± 0.001	11.307 ± 0.002	N/A ± N/A
J04352089+2254242	247592507	68.83708944	22.90673722	10.10	-14.50	13.30	N/A ± N/A	N/A ± N/A	N/A ± N/A	N/A ± N/A	N/A ± N/A	N/A ± N/A
J04352474+2426218	247804500	68.853103	24.439415	12.00	-36.00	17.06	N/A ± N/A	N/A ± N/A	N/A ± N/A	N/A ± N/A	N/A ± N/A	N/A ± N/A
J04352737+2414589	247776947	68.86404417	24.24966056	4.50	-21.70	11.86	15.613 ± 0.006	13.563 ± 0.002	11.903 ± 0.001	11.168 ± 0.001	11.081 ± 0.002	N/A ± N/A
J04354733+2250216	247583818	68.94722333	22.83936806	11.80	-13.20	11.86	N/A ± N/A	N/A ± N/A	N/A ± N/A	N/A ± N/A	N/A ± N/A	N/A ± N/A
J04355277+2254231	247592463	68.96991611	22.90643861	-4.50	-11.20	13.41	N/A ± N/A	N/A ± N/A	N/A ± N/A	N/A ± N/A	N/A ± N/A	N/A ± N/A
J04355349+2254089	247591948	68.97290556	22.90250056	-10.60	-24.80	13.88	N/A ± N/A	N/A ± N/A	N/A ± N/A	N/A ± N/A	N/A ± N/A	N/A ± N/A
J04355415+2254134	247592103	68.97562917	22.90375806	10.80	-15.40	10.78	N/A ± N/A	N/A ± N/A	N/A ± N/A	N/A ± N/A	N/A ± N/A	6.389 ± 0.269
J04372686+1851268	247119725	69.36196778	18.85741111	19.50	-36.90	11.23	16.577 ± 0.009	15.851 ± 0.012	15.125 ± 0.011	14.293 ± 0.011	14.334 ± 0.016	N/A ± N/A
J04381304+2022471	247280905	69.55436889	20.37972667	2.00	-7.90	12.03	15.582 ± 0.007	12.935 ± 0.001	11.909 ± 0.001	11.513 ± 0.001	11.655 ± 0.003	N/A ± N/A
J04381561+2302276	247609913	69.56504667	23.04099806	-6.50	-15.30	13.24	17.642 ± 0.012	15.588 ± 0.007	13.312 ± 0.002	12.5 ± 0.002	12.445 ± 0.01	N/A ± N/A
J04382858+2610494	248049475	69.61910667	26.17988861	0.00	0.00	13.21	15.598 ± 0.008	15.697 ± 0.012	15.544 ± 0.013	14.482 ± 0.013	13.891 ± 0.018	N/A ± N/A
J04391741+2247533	247578338	69.82258194	22.79815944	12.70	-9.00	12.72	N/A ± N/A	N/A ± N/A	N/A ± N/A	N/A ± N/A	N/A ± N/A	N/A ± N/A
J04391779+2221034	247520207	69.82414528	22.35094389	8.30	-14.80	11.63	15.362 ± 0.007	15.464 ± 0.011	10.344 ± 0.001	13.74 ± 0.008	10.142 ± 0.001	N/A ± N/A
J04410470+2451062	247864498	70.269635	24.85171056	4.80	-19.90	12.23	16.265 ± 0.008	13.509 ± 0.001	12.014 ± 0.001	11.214 ± 0.001	10.994 ± 0.002	N/A ± N/A
J04412400+2715124	248175684	70.34999111	27.25347556	3.60	5.00	12.87	N/A ± N/A	N/A ± N/A	N/A ± N/A	N/A ± N/A	N/A ± N/A	N/A ± N/A
J04412472+2554484	248014510	70.35300833	25.91346333	1.30	-2.10	10.24	15.693 ± 0.009	11.69 ± 0.001	10.168 ± 0.001	9.263 ± 0.001	9.651 ± 0.003	2.523 ± 0.406
J04415515+2658495	248145565	70.47980861	26.98039361	-0.69	-21.30	9.69	N/A ± N/A	N/A ± N/A	N/A ± N/A	N/A ± N/A	N/A ± N/A	9.314 ± 0.226
J04420548+2522562	247941378	70.52288944	25.38246222	2.90	-10.90	14.17	18.277 ± 0.017	16.13 ± 0.004	14.35 ± 0.011	13.033 ± 0.001	11.946 ± 0.004	N/A ± N/A
J04420732+2523032	247941613	70.53054389	25.38423111	1.00	-28.10	14.57	18.478 ± 0.019	16.463 ± 0.004	14.363 ± 0.003	15.687 ± 0.014	11.669 ± 0.004	N/A ± N/A
J04420777+2523118	247941930	70.53241139	25.38659222	5.30	-9.20	14.31	18.298 ± 0.015	16.031 ± 0.004	14.119 ± 0.01	16.482 ± 0.015	11.935 ± 0.004	N/A ± N/A
J04442685+1952169	247225984	71.11188194	19.87136611	36.90	-38.90	12.08	N/A ± N/A	N/A ± N/A	N/A ± N/A	N/A ± N/A	N/A ± N/A	N/A ± N/A
J04445445+2717454	248180268	71.22690167	27.29590389	7.20	-22.60	9.46	N/A ± N/A	N/A ± N/A	N/A ± N/A	N/A ± N/A	N/A ± N/A	N/A ± N/A
J04464475+2224508	247528573	71.68647833	22.41412833	0.20	-3.50	12.75	16.321 ± 0.008	15.548 ± 0.012	12.819 ± 0.002	12.262 ± 0.001	12.354 ± 0.008	N/A ± N/A
J04465327+2255128	247594260	71.7219625	22.92026278	33.20	-15.80	12.44	16.545 ± 0.01	16.37 ± 0.019	12.397 ± 0.001	11.643 ± 0.001	11.749 ± 0.002	N/A ± N/A
J04500019+2229575	247539775	72.50082778	22.4992925	0.60	-17.60	11.17	15.296 ± 0.01	11.69 ± 0.001	10.959 ± 0.001	10.692 ± 0.001	10.897 ± 0.002	8.506 ± 0.248
J04504608+2126535	247406403	72.69201583	21.44821	-3.00	-4.30	11.50	15.963 ± 0.009	12.865 ± 0.001	11.502 ± 0.001	11.027 ± 0.001	11.351 ± 0.003	N/A ± N/A
J05080709+2427123	247806504	77.02959806	24.45343444	-11.00	-15.90	15.35	N/A ± N/A	N/A ± N/A	N/A ± N/A	N/A ± N/A	N/A ± N/A	N/A ± N/A

NOTES

References: u'g'r'i'z' are from Alam et al. (2015), ¹Gaia Collaboration et al. (2016) Gaia DR1 <http://gea.esac.esa.int/archive/>

TABLE 2

2MASS ID	J mag ^{1,2}	H mag ^{1,2}	K mag ^{1,2}	WISE 1 ³	WISE 2 ³	WISE 3 ³	WISE 4 ³
J04222908+1922298	9.306 ± 0.02	8.894 ± 0.026	8.783 ± 0.017	8.729 ± 0.023	8.781 ± 0.019	8.714 ± 0.03	8.13 ± 0.277
J04270280+2542223	8.171 ± 0.026	7.256 ± 0.023	6.734 ± 0.024	6.028 ± 0.114	5.23 ± 0.068	3.829 ± 0.014	2.27 ± 0.024
J04274793+2430121	9.612 ± 0.022	9.273 ± 0.024	9.061 ± 0.018	8.928 ± 0.022	8.896 ± 0.021	8.92 ± 0.048	8.647 ± N/A
J04294230+2608417	9.594 ± 0.022	9.26 ± 0.019	9.106 ± 0.017	9.019 ± 0.023	9.013 ± 0.021	8.993 ± 0.044	8.098 ± N/A
J04295156+2606448	9.415 ± 0.02	8.417 ± 0.023	7.779 ± 0.023	7.27 ± 0.037	6.729 ± 0.023	4.906 ± 0.016	2.97 ± 0.016
J04302961+2426450	9.388 ± 0.024	8.398 ± 0.018	7.924 ± 0.016	7.4 ± 0.033	6.982 ± 0.02	5.133 ± 0.019	3.193 ± 0.029
J04303292+2602440	11.327 ± 0.021	10.92 ± 0.022	10.809 ± 0.023	10.722 ± 0.022	10.753 ± 0.021	10.814 ± 0.232	8.188 ± N/A
J04304153+2430416	10.216 ± 0.022	9.603 ± 0.022	9.375 ± 0.018	9.231 ± 0.023	9.197 ± 0.02	9.191 ± 0.044	8.89 ± N/A
J04304425+2601244	8.719 ± 0.03	7.758 ± 0.024	7.096 ± 0.016	6.12 ± 0.104	5.314 ± 0.055	3.599 ± 0.011	1.8 ± 0.012
J04305137+2442222	9.495 ± 0.021	8.695 ± 0.029	8.441 ± 0.021	8.106 ± 0.022	7.703 ± 0.021	5.96 ± 0.015	4.319 ± 0.024
J04305171+2441475	12.842 ± 0.023	11.435 ± 0.026	10.314 ± 0.023	8.56 ± 0.021	7.076 ± 0.021	4.449 ± 0.014	1.909 ± 0.016
J04311686+2150252	9.24 ± 0.034	8.83 ± 0.03	8.734 ± 0.02	8.673 ± 0.022	8.705 ± 0.019	8.631 ± 0.034	8.306 ± 0.376
J04314963+2553067	8.697 ± 0.02	8.431 ± 0.018	8.367 ± 0.027	8.323 ± 0.023	8.347 ± 0.02	8.32 ± 0.036	7.909 ± 0.324
J04321786+2422149	11.539 ± 0.02	10.791 ± 0.02	10.382 ± 0.02	10.092 ± 0.023	9.769 ± 0.02	9.556 ± 0.075	8.147 ± N/A
J04321885+2422271	9.538 ± 0.02	8.432 ± 0.021	8.106 ± 0.021	7.911 ± 0.026	7.829 ± 0.02	7.716 ± 0.023	7.659 ± 0.251
J04324282+2552314	N/A ± N/A	N/A ± N/A	N/A ± N/A	N/A ± N/A	N/A ± N/A	N/A ± N/A	N/A ± N/A
J04324303+2552311	9.136 ± N/A	8.117 ± N/A	7.354 ± 0.033	6.252 ± 0.079	5.476 ± 0.045	3.69 ± 0.012	1.802 ± 0.016
J04330664+2409549	8.146 ± 0.023	7.357 ± 0.026	6.96 ± 0.016	6.473 ± 0.076	6.023 ± 0.026	5.181 ± 0.016	2.885 ± 0.021
J04331003+2433433	9.325 ± 0.021	8.613 ± 0.016	8.422 ± 0.021	8.412 ± 0.023	8.38 ± 0.02	8.264 ± 0.031	8.329 ± 0.368
J04332887+2416456	7.119 ± 0.018	7.006 ± 0.017	6.946 ± 0.017	6.907 ± 0.055	6.937 ± 0.021	6.999 ± 0.021	6.809 ± 0.117
J04333405+2421170	9.341 ± 0.02	8.418 ± 0.021	7.888 ± 0.023	7.087 ± 0.106	6.35 ± 0.072	4.011 ± 0.016	2.27 ± 0.027
J04333456+2421058	9.053 ± 0.027	8.108 ± 0.026	7.468 ± 0.021	6.568 ± 0.138	5.899 ± 0.093	3.84 ± 0.014	1.803 ± 0.016
J04335200+2250301	9.48 ± 0.02	8.431 ± 0.04	7.793 ± 0.02	6.756 ± 0.068	6.032 ± 0.038	4.367 ± 0.014	2.412 ± 0.026
J04335470+2613275	9.866 ± 0.025	8.591 ± 0.036	7.86 ± 0.026	7.396 ± 0.032	6.824 ± 0.02	5.252 ± 0.014	3.569 ± 0.025
J04335562+2425016	10.056 ± 0.02	9.286 ± 0.022	9.003 ± 0.017	8.854 ± 0.023	8.836 ± 0.02	8.789 ± 0.037	8.016 ± N/A
J04340717+2251227	9.606 ± 0.022	9.018 ± 0.04	8.755 ± 0.018	8.643 ± 0.023	8.624 ± 0.021	8.597 ± 0.03	8.38 ± N/A
J04342961+2423421	10.748 ± 0.022	10.339 ± 0.023	10.208 ± 0.018	10.095 ± 0.024	10.08 ± 0.021	10.143 ± 0.088	8.218 ± N/A
J04345017+2414403	7.425 ± 0.023	7.21 ± 0.02	7.111 ± 0.023	7.044 ± 0.051	7.023 ± 0.019	7.089 ± 0.019	6.981 ± 0.11
J04345542+2428531	9.433 ± 0.024	8.546 ± 0.023	8.047 ± 0.024	7.447 ± 0.036	6.76 ± 0.02	4.645 ± 0.014	2.505 ± 0.022
J04352089+2254242	9.781 ± 0.022	8.933 ± 0.024	8.592 ± 0.018	8.454 ± 0.023	8.403 ± 0.019	8.298 ± 0.026	8.453 ± 0.474
J04352474+2426218	14.576 ± 0.031	13.887 ± 0.037	13.788 ± 0.044	13.477 ± 0.028	13.352 ± 0.034	12.092 ± 0.439	8.966 ± 0.523
J04352737+2414589	9.139 ± 0.021	8.342 ± 0.027	8.015 ± 0.021	7.657 ± 0.029	7.216 ± 0.02	5.166 ± 0.016	3.039 ± 0.022
J04354733+2250216	8.655 ± 0.024	7.731 ± 0.016	7.135 ± 0.021	6.633 ± 0.071	5.415 ± 0.037	3.485 ± 0.015	1.51 ± 0.021
J04355277+2254231	9.549 ± 0.022	8.469 ± 0.065	7.625 ± 0.024	6.018 ± 0.057	5.733 ± 0.044	3.636 ± 0.016	1.431 ± 0.019
J04355349+2254089	10.041 ± 0.023	9.154 ± 0.022	8.797 ± 0.021	8.614 ± 0.033	8.547 ± 0.031	8.296 ± 0.032	8.189 ± N/A
J04355415+2254134	8.103 ± 0.02	7.489 ± 0.036	7.234 ± 0.016	7.118 ± 0.046	7.068 ± 0.026	6.849 ± 0.023	4.512 ± 0.046
J04372686+1851268	9.422 ± 0.041	8.558 ± 0.036	8.666 ± 0.054	8.691 ± 0.045	8.685 ± 0.044	8.543 ± 0.048	7.465 ± N/A
J04381304+2022471	10.074 ± 0.023	9.534 ± 0.023	9.358 ± 0.018	9.218 ± 0.022	9.262 ± 0.021	9.244 ± 0.039	8.15 ± N/A
J04381561+2302276	10.623 ± 0.023	9.931 ± 0.022	9.769 ± 0.021	9.661 ± 0.023	9.621 ± 0.02	9.551 ± 0.051	8.581 ± 0.389
J04382858+2610494	9.47 ± 0.022	8.243 ± 0.033	7.303 ± 0.017	6.341 ± 0.097	5.428 ± 0.053	3.48 ± 0.013	1.168 ± 0.014
J04391741+2247533	9.97 ± 0.023	9.26 ± 0.021	8.958 ± 0.02	8.591 ± 0.023	8.189 ± 0.021	6.227 ± 0.017	4.722 ± 0.028
J04391779+2221034	9.424 ± 0.02	8.6 ± 0.018	8.163 ± 0.018	7.504 ± 0.028	7.207 ± 0.019	5.696 ± 0.015	3.565 ± 0.022
J04410470+2451062	9.244 ± 0.022	8.479 ± 0.02	8.275 ± 0.026	8.213 ± 0.025	8.115 ± 0.02	8.012 ± 0.022	7.817 ± 0.22
J04412400+2715124	11.037 ± 0.022	10.568 ± 0.021	10.428 ± 0.02	10.351 ± 0.023	10.358 ± 0.02	10.375 ± 0.097	8.797 ± N/A
J04412472+2554484	6.994 ± 0.02	6.461 ± 0.033	6.169 ± 0.023	6.068 ± 0.114	5.849 ± 0.043	6.042 ± 0.016	5.88 ± 0.052
J04415515+2658495	8.365 ± 0.03	8.068 ± 0.017	7.973 ± 0.029	7.931 ± 0.026	7.952 ± 0.019	7.939 ± 0.02	7.782 ± 0.236
J04420548+2522562	9.787 ± 0.022	8.663 ± 0.034	8.227 ± 0.02	7.978 ± 0.024	7.776 ± 0.021	7.426 ± 0.018	6.218 ± 0.057
J04420732+2523032	9.58 ± 0.023	8.401 ± 0.024	7.945 ± 0.023	6.914 ± 0.019	5.378 ± 0.01	2.626 ± 0.006	3.046 ± 0.009
J04420777+2523118	9.811 ± 0.022	8.601 ± 0.021	7.942 ± 0.016	6.735 ± 0.034	6.322 ± 0.02	4.506 ± 0.013	2.747 ± 0.017
J04442685+1952169	9.563 ± 0.032	8.881 ± 0.04	8.707 ± 0.027	8.483 ± 0.022	8.464 ± 0.02	8.38 ± 0.024	8.145 ± 0.256
J04445445+2717454	7.734 ± 0.023	7.281 ± 0.036	7.154 ± 0.021	7.028 ± 0.048	7.046 ± 0.019	7.029 ± 0.019	6.878 ± 0.103
J04464475+2224508	10.52 ± 0.021	9.9 ± 0.022	9.728 ± 0.017	9.654 ± 0.023	9.704 ± 0.02	9.536 ± 0.046	8.395 ± N/A
J04465327+2255128	9.875 ± 0.022	9.234 ± 0.022	9.024 ± 0.018	8.942 ± 0.024	8.921 ± 0.021	8.838 ± 0.03	8.482 ± 0.486
J04500019+2229575	9.503 ± 0.024	9.021 ± 0.023	8.887 ± 0.018	8.819 ± 0.023	8.819 ± 0.02	8.729 ± 0.025	8.325 ± 0.276
J04504608+2126535	9.438 ± 0.022	8.861 ± 0.022	8.704 ± 0.017	8.634 ± 0.025	8.692 ± 0.023	8.601 ± 0.03	8.213 ± N/A
J05080709+2427123	11.396 ± 0.022	10.701 ± 0.022	10.481 ± 0.018	10.279 ± 0.023	10.104 ± 0.021	9.293 ± 0.036	5.561 ± 0.044

NOTES

References: ¹Cutri et al. (2003), ²Skrutskie et al. (2006), ³Cutri & et al. (2014)

TABLE 3

2MASS ID	Stetson J	Stetson H	RMS	$\Delta 90$	Variable ^a	Blend ^b	Classification ^c	Period	$\frac{\text{PeakPower}}{\text{SimulatedPower}}$ ^d	Amplitude ^e (Mag)
J04222908+1922298	0.355	0.207	0.018	0.058	0	0	Periodic	14.810	20.33	0.0052
J04270280+2542223	7.349	5.063	0.187	0.605	1	0	Periodic	16.504	19.77	0.0500
J04274793+2430121	0.046	0.016	0.020	0.065	0	0	N/A	N/A	N/A	N/A
J04294230+2608417	0.116	0.070	0.019	0.062	0	0	Periodic	0.952	8.90	0.0017
J04295156+2606448	3.412	2.286	0.377	1.221	1	0	Dipper/Periodic	1.180	21.44	0.1010
J04302961+2426450	1.148	0.774	0.123	0.399	1	0	Periodic	1.026	35.41	0.0297
J04303292+2602440	0.258	0.129	0.108	0.350	0	0	Blend	N/A	6.42	N/A
J04304153+2430416	0.035	0.022	0.048	0.155	0	0	N/A	N/A	N/A	N/A
J04304425+2601244	10.724	7.233	0.420	1.319	1	0	Dipper/Periodic	4.086	33.10	0.1208
J04305137+2442222	0.218	0.150	0.091	0.295	0	1	Periodic	1.311	14.16	0.0113
J04305171+2441475	0.218	0.150	0.091	0.295	0	1	Blend	N/A	N/A	N/A
J04311686+2150252	2.193	1.467	0.050	0.167	1	0	Periodic	1.593	63.22	0.0249
J04314963+2553067	0.974	0.350	0.013	0.044	0	0	Periodic	0.967	44.83	0.0026
J04321786+2422149	0.138	0.088	0.053	0.175	0	1	Blend	N/A	N/A	N/A
J04321885+2422271	0.138	0.088	0.053	0.175	0	1	Periodic	1.661	4.15	0.0056
J04324282+2552314	2.807	1.698	0.144	0.486	1	1	Blend	N/A	N/A	N/A
J04324303+2552311	2.807	1.698	0.144	0.486	1	1	Periodic	1.055	23.18	0.0440
J04330664+2409549	3.862	2.588	0.062	0.198	1	0	Dipper/Periodic	0.809	44.71	0.0143
J04331003+2433433	1.343	0.939	0.058	0.196	1	0	Periodic	2.743	196.47	0.0499
J04332887+2416456	2.758	0.206	0.012	0.040	0	0	Periodic	0.516	12.11	0.0020
J04333405+2421170	6.008	4.003	0.168	0.525	1	1	Dipper	N/A	N/A	N/A
J04333456+2421058	6.008	4.003	0.168	0.525	1	1	Blend	N/A	N/A	N/A
J04335200+2250301	1.612	1.101	0.126	0.423	1	0	N/A	N/A	N/A	N/A
J04335470+2613275	0.421	0.275	0.172	0.562	1	0	Periodic	2.751	16.98	0.0573
J04335562+2425016	0.055	0.028	0.075	0.243	0	0	N/A	N/A	N/A	N/A
J04340717+2251227	0.094	0.059	0.036	0.118	0	0	Periodic	1.177	3.68	0.0044
J04342961+2423421	0.030	0.016	0.068	0.221	0	0	N/A	N/A	N/A	N/A
J04345017+2414403	0.807	0.283	0.008	0.026	0	0	Periodic	0.957	20.20	0.0012
J04345542+2428531	16.883	11.315	0.929	2.785	1	0	Dipper/Periodic	13.613	141.18	0.2628
J04352089+2254242	0.034	0.022	0.124	0.397	0	0	N/A	N/A	N/A	N/A
J04352474+2426218	0.087	0.053	0.055	0.178	0	0	Periodic	0.929	5.78	0.0042
J04352737+2414589	1.203	0.750	0.066	0.221	1	0	Periodic	1.184	43.23	0.0280
J04354733+2250216	8.693	5.085	0.374	1.240	1	0	UXor	N/A	N/A	N/A
J04355277+2254231	2.155	1.391	0.035	0.117	1	1	Blend	N/A	N/A	N/A
J04355349+2254089	2.155	1.391	0.035	0.117	1	1	Blend	N/A	N/A	N/A
J04355415+2254134	2.155	1.391	0.035	0.117	1	1	Periodic	5.798	31.04	0.0130
J04372686+1851268	1.047	0.713	0.043	0.139	1	0	Periodic	1.310	31.72	0.0212
J04381304+2022471	0.413	0.238	0.048	0.155	0	0	Periodic	2.935	29.67	0.0109
J04381561+2302276	0.099	0.061	0.108	0.353	0	0	Periodic	1.184	5.12	0.0155
J04382858+2610494	3.219	2.268	0.306	0.994	1	0	Periodic	0.961	23.53	0.0707
J04391741+2247533	1.303	0.896	0.192	0.654	1	0	Periodic	5.454	30.36	0.0510
J04391779+2221034	2.794	1.877	0.035	0.114	1	0	Periodic	5.765	28.27	0.0118
J04410470+2451062	0.983	0.695	0.069	0.224	1	0	Periodic	0.844	66.23	0.0339
J04412400+2715124	0.084	0.044	0.072	0.232	0	0	Periodic	0.601	5.89	0.0063
J04412472+2554484	0.718	0.343	0.014	0.046	0	0	Periodic	20.121	56.80	0.0025
J04415515+2658495	2.990	1.933	0.025	0.081	1	0	Periodic	0.965	69.91	0.0067
J04420548+2522562	1.511	1.041	0.135	0.443	1	1	Periodic	23.935	16.09	0.0301
J04420732+2523032	1.511	1.041	0.135	0.443	1	1	Periodic	23.935	16.09	0.0301
J04420777+2523118	1.511	1.041	0.135	0.443	1	1	Periodic	23.935	16.09	0.0301
J04442685+1952169	0.093	0.059	0.043	0.142	0	0	Periodic	12.594	4.60	0.0057
J04445445+2717454	5.744	4.258	0.037	0.122	1	0	N/A	N/A	N/A	N/A
J04464475+2224508	0.074	0.049	0.071	0.232	0	0	Periodic	0.517	4.65	0.0081
J04465327+2255128	0.289	0.185	0.055	0.180	1	0	Periodic	3.766	25.13	0.0169
J04500019+2229575	1.925	1.283	0.070	0.233	1	0	Periodic	11.198	48.06	0.0243
J04504608+2126535	0.094	0.046	0.027	0.087	0	0	N/A	N/A	N/A	N/A
J05080709+2427123	0.068	0.044	0.016	0.054	0	0	Periodic	45.496	3.59	0.0014

NOTES

^aA star was flagged as a variable if it passed a 2σ cut on the rms and $\Delta 90$ statistic, a 3σ cut on J , and a 5σ cut on L . See section 4.1 for a description of how the cuts were determined.

^bIf another star is within $2'$ and 1.5 magnitude of the target, it is classified as a blend.

^cAny target classified as "N/A" did not show a periodic signal or any variability that would classify it as a dipper or UXor.

^dA measurement of how much larger the Lomb-Scargle peak of the actual period is versus the maximum peak of the 1000 simulated light curves. Any period where this ratio is >1 is defined as a real period.

^eFor any target classified as "N/A" the reported amplitude is the $\Delta 90$ statistic that identifies the magnitude range for 90% of the data points.